UCID--21362-Vol.1

DE90 006335

# Survey of Degradation Modes of Candidate Materials for High-Level Radioactive-Waste Disposal Containers

Volume 1
Phase Stability

D. B. Bullen and G. E. Gdowski
Science & Engineering Associates, Inc.
Pleasanton, Calif.

August 1988



LAWRENCE LIVERMORE NATIONAL LABORATORY
University of California • Livermore, California • 94550

# Contents

# List of Volumes of the Survey

This is Volume 1 of the report *Survey of Degradation Modes of Candidate Materials for High-Level Radioactive-Waste Disposal Containers*. The titles of all of the volumes are as follows:

Overview
Volume 1: Phase Stability
Volume 2: Oxidation and Corrosion
Volume 3: Localized Corrosion and Stress Corrosion Cracking of Austenitic Alloys
Volume 4: Stress Corrosion Cracking of Copper-Based Alloys
Volume 5: Localized Corrosion of Copper-Based Alloys
Volume 6: Effects of Hydrogen in Austenitic and Copper-Based Alloys
Volume 7: Weldability of Austenitic Alloys
Volume 8: Weldability of Copper-Based Alloys

# Acronyms

| | |
|---|---|
| bcc | body-centered cubic |
| BWR | boiling-water reactor |
| CHLW | commercial high-level waste |
| CDA | Copper Development Association |
| DHLW | defense high-level waste |
| EDX | energy-dispersive x-ray analysis |
| fcc | face-centered cubic |
| hcp | hexagonal close-packed |
| IGSCC | intergranular stress corrosion cracking |
| NNWSI | Nevada Nuclear Waste Storage Investigations Project |
| NWMP | Nuclear Waste Management Program |
| OFHC | oxygen-free, high-conductivity |
| PWR | pressurized-water reactor |
| TTP | time-temperature precipitation |

# Executive Summary

This volume discusses the phase stability of the six candidate materials for the metal containers to be used in disposing of high-level radioactive waste. Three of the candidates are iron- to nickel-based austenitic materials: Type 304L stainless steel, Type 316L stainless steel, and Alloy 825. The other three are copper-based alloys: CDA 102 (oxygen-free copper), CDA 613 (Cu-7Al), and CDA 715 (Cu-30Ni). These materials, particularly the copper alloys, are used extensively in marine environments. The austenitic alloys are used extensively in the nuclear industry.

Radioactive waste will include spent fuel assemblies from reactors and borosilicate glass forms, and will be sent to the prospective repository in Yucca Mountain, Nevada, for disposal. Disposal containers can undergo several forms of degradation in the repository during their lifetimes. The selection of the candidate material that is adequate for repository conditions will be based on three tasks: a survey of the literature, corrosion testing, and predictions from modeling. Lawrence Livermore National Laboratory has responsibility for all three. This volume surveys the literature on the phase stability of the candidate materials. Other volumes in the survey address the effects of hydrogen; general oxidation and corrosion; localized corrosion; stress corrosion cracking; and the effects of welding.

This volume is divided into two parts. The first discusses the phase stability of the austenitic alloys, and the second addresses the phase stability of the copper-based alloys.

Section 1 is an introduction to the high-level radioactive-waste project at Yucca Mountain. Shortly after emplacement of the containers in the repository, radioactive decay of the stored waste will result in substantial heat transfer to the surroundings and in emission of gamma radiation. The temperature of most of the containers is expected to reach 250°C within a few years of emplacement and then slowly decrease. Container temperatures are expected to remain above 100°C for least 300 yr.

Sections 2 through 4 address the phase stability of the austenitic candidate alloys. Types 304L and 316L stainless steels have been identified as metastable materials under repository-relevant conditions. Metastability is defined as nonequilibrium phase formation due to kinetic limitations. Diffusion processes that permit precipitation are severely limited at repository temperatures. Alloy 825 appears to be stable under repository conditions.

Carbide precipitation has been identified in all of the austenitic candidate alloys and can cause sensitization of these alloys. Sensitization is the enhanced susceptibility to intergranular stress corrosion cracking. The carbides involved have been identified as $M_{23}C_6$. In Types 304L and 316L stainless steels, the metallic component is primarily chromium. In Alloy 825, both chromium and titanium precipitate, and the composition is a function of precipitation time and temperature. Increased titanium content in these precipitates limits chromium depletion near the precipitate and preserves the resistance of the alloy to corrosion.

Intermetallic-phase formation is seen in Type 316L stainless steel. The intermetallic phases include $\sigma$, $\chi$, and Laves phases. The formation of $\sigma$ phase has been shown to significantly reduce the impact strength of austenitic alloys because of its hard, brittle microstructure. No intermetallic-phase formation has been documented for Alloy 825.

Sections 5 through 7 discuss the phase stability of the copper-based alloys. According to the available experimental data, all of these candidate materials are single-phased to at least 300°C. Intermetallic iron particles are present in CDA 613, but with proper processing, these particles are dispersed throughout the alloy. The slow diffusion of constituent species severely limits the study of equilibrium phases at low temperatures. For CDA 715, there is a proposed two-phase region for temperatures less than 200°C. Diffusion rates are extremely low at these temperatures, and the proposed phase separation probably would not occur even during the required container lifetime. More detailed consideration of this concern may be prudent.

The precipitation of the minor constituent alloying species in the copper-based alloys is also discussed. In particular, manganese, iron, tin, and phosphorus are considered in the appropriate alloys. Manganese is soluble in copper at its concentrations in the candidate alloys. Although iron is not soluble at any concentration in copper, it remains in solution because of its slow diffusion rate or the formation of intermetallic compounds. Tin and phosphorus are partially soluble at the higher repository

temperatures. Section 5 gives diffusion data that may be necessary to determine whether precipitation of iron or tin would occur.

On the basis of consideration of phase stability, the austenitic materials are ranked as follows: Alloy 825 (best), Type 316L stainless steel, and then Type 304L stainless steel (worst). For the copper-based materials CDA 102 (oxygen-free copper) is best, and both CDA 715 and CDA 613 are considered equally less stable materials.

# Survey of Degradation Modes of Candidate Materials for High-Level Radioactive-Waste Disposal Containers

## Volume 1: Phase Stability


## Abstract

Three copper-based alloys and three iron- to nickel-based austenitic alloys are being considered as possible materials for fabrication of high-level radioactive-waste disposal containers. The waste will include spent fuel assemblies from reactors as well as high-level waste in borosilicate glass and will be sent to the prospective site at Yucca Mountain, Nevada, for disposal. The copper-based alloy materials are CDA 102 (oxygen-free copper), CDA 613 (Cu-7Al), and CDA 715 (Cu-30Ni). The austenitic materials are Types 304L and 316L stainless steels and Alloy 825. The waste-package containers must maintain substantially complete containment for at least 300 yr and perhaps as long as 1000 yr, and they must be retrievable from the disposal site during the first 50 yr after emplacement. The containers will be exposed to high temperatures and high gamma radiation fields from the decay of high-level waste.

This volume surveys the available data on the phase stability of both groups of candidate alloys. The austenitic alloys are reviewed in terms of the physical metallurgy of the iron-chromium-nickel system, martensite transformations, carbide formation, and intermetallic-phase precipitation. The copper-based alloys are reviewed in terms of their phase equilibria and the possibility of precipitation of the minor alloying constituents.

For the austenitic materials, the ranking based on phase stability is: Alloy 825 (best), Type 316L stainless steel, and then Type 304L stainless steel (worst). For the copper-based materials, the ranking is: CDA 102 (oxygen-free copper) (best), and then both CDA 715 and CDA 613.


## 1. Introduction

The Nuclear Waste Management Program (NWMP) at Lawrence Livermore National Laboratory is responsible for developing the waste-package design to meet the Nuclear Regulatory Commission's licensing requirements for the Nevada Nuclear Waste Storage Investigations (NNWSI) Project. Waste will include (1) spent fuel from civilian nuclear power plants, namely, fuel assemblies and consolidated fuel pins from pressurized-water reactors (PWRs) and boiling-water reactors (BWRs), (2) commercial high-level waste (CHLW) in the form of borosilicate glass in which commercial spent-fuel reprocessing wastes are incorporated, and (3) defense high-level waste (DHLW), also incorporated in borosilicate glass.

The waste package is being designed for emplacement in the Topopah Spring Member of the Paintbrush Tuff at the Yucca Mountain site in Nevada. The reference horizon is located 350 m below the ground surface and 200 m above the static water table. The compositions of the vadose water and gas phase present make the repository conditions slightly oxidizing.

The Metal Barrier Selection and Testing Task of the NNWSI Project is responsible for the selection of the materials to be employed in the waste-package container. Six candidate materials are currently under consideration. These materials include three iron- to nickel-based austenitic materials and three copper-based alloys. The

austenitic materials are Type 304L stainless steel, Type 316L stainless steel, and Alloy 825. The copper-based alloys are CDA 102 (oxygen-free copper), CDA 613 (Cu-7Al), and CDA 715 (Cu-30Ni). One of the criteria for the selection of the final metal barrier material is the stability of these materials in the repository environment.

The design criteria for the metal barrier require that the waste container maintain mechanical integrity for a period of approximately 50 yr after emplacement to permit retrieval of the nuclear waste during the preclosure phase of repository operation. The engineered barrier system is required to provide substantially complete containment of the waste for a period of 300 to 1000 yr. During the containment period, the metal barrier will be exposed to a changing environment. A few years after emplacement, the surfaces of many of the containers will reach a maximum temperature of about 250°C. This temperature will decay to about 150°C within about 100 yr after emplacement. Other containers will not reach such high temperatures owing to lower heat output. The early time period will also include the highest gamma radiation field from the decay of the high-level waste. The phase stability of the container material over this time period will have an impact on the mechanical and corrosion behavior of the metal barrier. Changes in the microstructure can result in considerable reduction in the fracture strength of the material, which would be important if retrieval were necessary. For instance, in the austenitic materials, precipitation of carbides at grain boundaries can modify the local alloy composition, resulting in conditions favorable to intergranular stress corrosion cracking (IGSCC).

This volume is one of eight that make up the survey of degradation modes [1]. The purpose of the survey is to characterize the candidate materials. The other volumes in the survey address oxidation and corrosion, stress corrosion cracking, localized corrosion, effects of hydrogen, and effects of welding on container integrity.

This volume addresses the phase stability of the candidate materials. First, there is a discussion of the phase stability of the iron- to nickel-based austenitic candidate materials, and then there is a discussion of the phase stability of the copper-based candidate materials. Each discussion summarizes our review of the literature, highlighting areas in which significant data and results exist. Each also identifies areas in which very little data was found. Finally, the candidate materials in each group are ranked with respect to phase stability.

A discussion on the methodology and extent of the literature search can be found in the Overview.*

# 2. Austenitic Candidate Alloys

The austenitic alloys being considered are Type 304L stainless steel, Type 316L stainless steel, and Alloy 825. These alloys are candidate materials for the metal barrier in the NWMP because of their adequate strength and relatively good corrosion resistance. The typical composition of these alloys is presented in Table 1. For purposes of comparison, the compositions of Types 304 and 316 stainless steels are also given in Table 1.

The phase stability of these alloys under repository-relevant conditions is a critical issue which will have an impact on the long-term mechanical and corrosion properties of the metal barrier. This section addresses the issues of phase stability that exist for each of the austenitic candidate alloys. A review of possible phase transformations and the impact of these transformations on mechanical and corrosion properties is also presented.

## 2.1 Physical Metallurgy of the Iron-Chromium-Nickel System

A number of general review articles on the constitution and structure of stainless steels and austenites have been identified in the technical literature [e.g., 2–4]. A summary of these articles and a review of metallurgy relevant to repository conditions are provided here. The austenitic candidate materials are all derived from the ternary iron-chromium-nickel system. A review of the physical metallurgy of this system provides an

* J. C. Farmer, R. D. McCright, J. N. Kass, *Survey of Degradation Modes of Candidate Materials for High-Level Radioactive-Waste Disposal Containers, Overview*, Lawrence Livermore National Laboratory, Livermore, California, UCID-21362 Overview (1988).

Table 1. Elemental composition of the austenitic candidate alloys (wt%).

| Element | Stainless steels | | | | Alloy 825 |
|---|---|---|---|---|---|
| | 304 | 304L | 316 | 316L | |
| C | 0.08 | 0.03 max | 0.08 | 0.03 max | 0.05 max |
| Mn | 2.00 | 2.00 max | 2.00 | 2.00 max | 1.0 max |
| Si | 1.00 | 1.00 max | 1.00 | 1.00 max | 0.5 max |
| Cr | 18.0–20.0 | 18.0–20.0 | 16.0–18.0 | 16.0–18.0 | 19.5–23.5 |
| Ni | 8.0–10.5 | 8.0–12.0 | 10.0–14.0 | 10.0–14.0 | 38.0–46.0 |
| P | 0.045 | 0.045 max | 0.045 | 0.045 max | — |
| S | 0.03 | 0.03 max | 0.03 | 0.03 max | 0.03 max |
| Cu | — | — | — | — | 1.5–3.0 |
| Ti | — | — | — | — | 0.6–1.2 |
| N | 0.10 | 0.10 | 0.10 | 0.10 | — |
| Mo | — | — | 2.0–3.0 | 2.0–3.0 | 3.0 |
| Fe | Bal. | Bal. | Bal. | Bal. | Bal. |

informative introduction to the aspects of phase stability that are critical to understanding the long-term performance of these alloys.

The equilibrium phases encountered in this ternary system are dictated by the allotropic forms of iron, which can be identified in the chromium-iron binary phase diagram shown in Fig. 1 [5]. Between the melting point (1539°C) and about 1390°C, pure iron exists as a body-centered cubic (bcc) structure that is usually called delta ($\delta$) ferrite. From about 1390 to 910°C, iron is face-centered cubic (fcc). This phase is called austenite or the gamma phase ($\gamma$). Below 910°C, iron again becomes bcc with a structure identified as alpha ($\alpha$) ferrite. There is no obvious microstructural difference between $\delta$ and $\alpha$ ferrite. This convention of nomenclature has been adopted to allow distinction between the conditions of formation.

The addition of chromium to iron (up to about 7 wt%) reduces the temperature of both the bcc $\leftrightarrow$ fcc transformation points, as indicated at the left side of Fig. 1. Above 7% chromium, the temperature range over which austenite exists is gradually reduced. Above 13% chromium, no $\alpha$ to $\gamma$ transformation occurs and ferrite is stable at all temperatures. Hence, chromium is said to be a ferrite-forming element. Other elements commonly employed in stainless steels that behave similarly are molybdenum, silicon, aluminum, titanium, and niobium.

Austenitic stainless steels all contain more than 16% chromium. It is obvious from Fig. 1 that a chromium content of this magnitude in a binary iron-chromium alloy would produce an entirely ferritic material. In austenitic stainless steels, the effect of chromium is counteracted by the addition of nickel. Figure 2 shows the equilibrium phase diagram for the iron-nickel system [5]. The austenite-phase region is significantly increased by the addition of nickel to iron. Therefore, nickel is called an austenite-forming element. Manganese, cobalt, copper, nitrogen, and carbon can also be employed as austenite-forming elements in certain alloy applications.

## 2.2 Metastable Alloy Systems

The phase diagrams presented above represent the equilibrium conditions for these alloy systems. It should be noted that many alloy applications employ thermomechanical treatments that do not necessarily produce equilibrium states. The equilibrium phases may not form due to kinetic limitations during cooling. Hence, a metastable phase may be present at temperatures that are too low to permit formation of an equilibrium phase. This is the case for Types 304L and 316L stainless steels. The compositions of these alloys suggest that the ferrite phase should be in

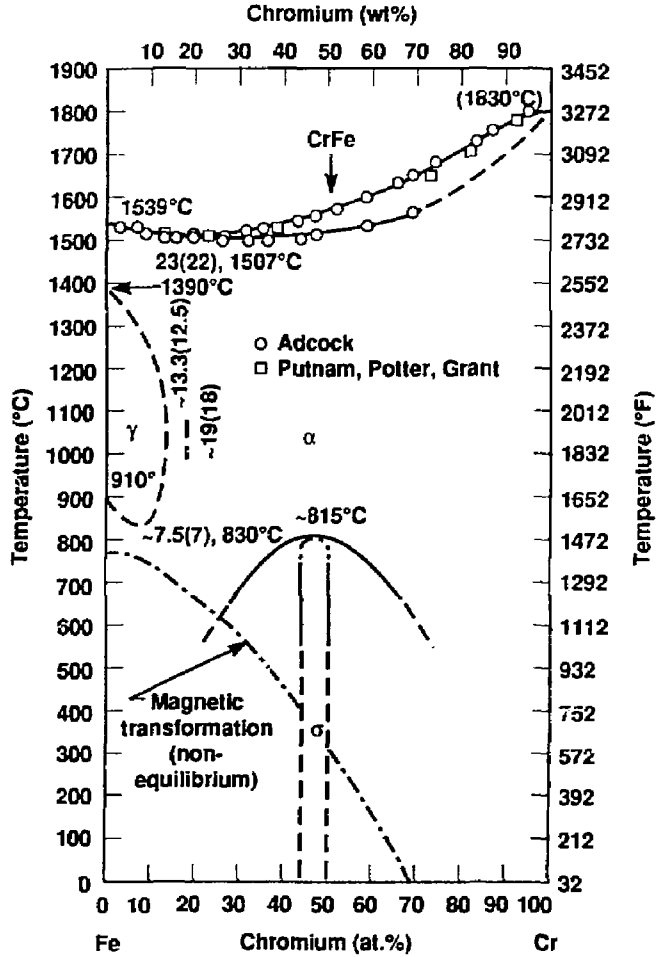


**Figure 1. Chromium-iron binary equilibrium phase diagram [5].**

equilibrium with the austenite phase at temperatures around 200°C. However, the diffusion processes that permit the precipitation of the ferrite phase are severely limited at this low temperature. This results in the production of an alloy that has an austenitic microstructure that is stable for reasonable engineering lifetimes (10 to 40 yr). The stability of these alloys over the considerably longer time periods of interest in the repository (up to 1000 yr) is addressed in later sections of this report.

Once an understanding is obtained of the effects of alloy additions to pure iron, it is a logical step to consider the ternary iron-chromium-nickel system in order to more fully comprehend the complex equilibrium phases present in stainless steels. Iron-chromium-nickel ternary phase diagrams for elevated temperatures are shown in Fig. 3. These diagrams show the equilibrium phase fields formed for various alloy compositions in the temperature range usually employed for austenitic stainless steel annealing. The annealing usually dissolves the constituents that are present. The alloys are quenched after the annealing.

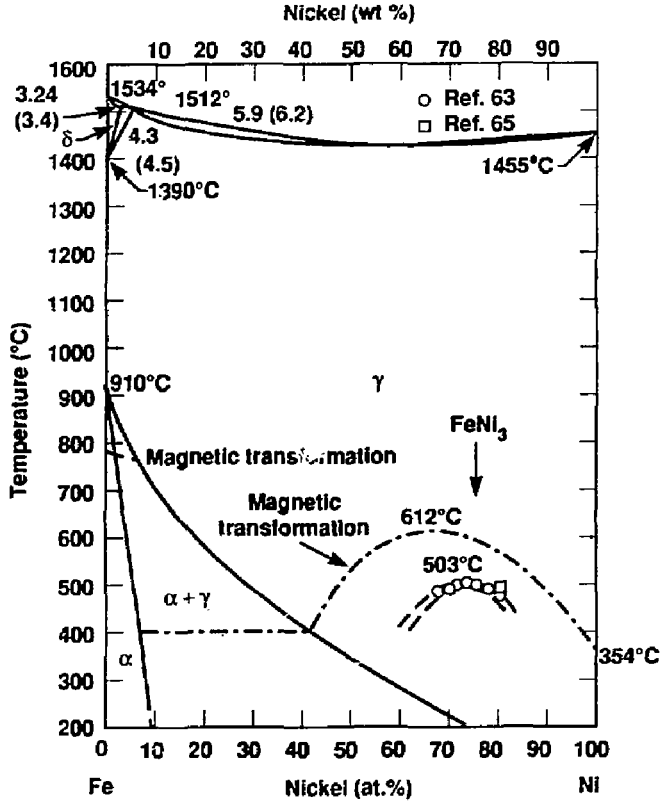


Figure 2. Iron-nickel binary equilibrium phase diagram [5].

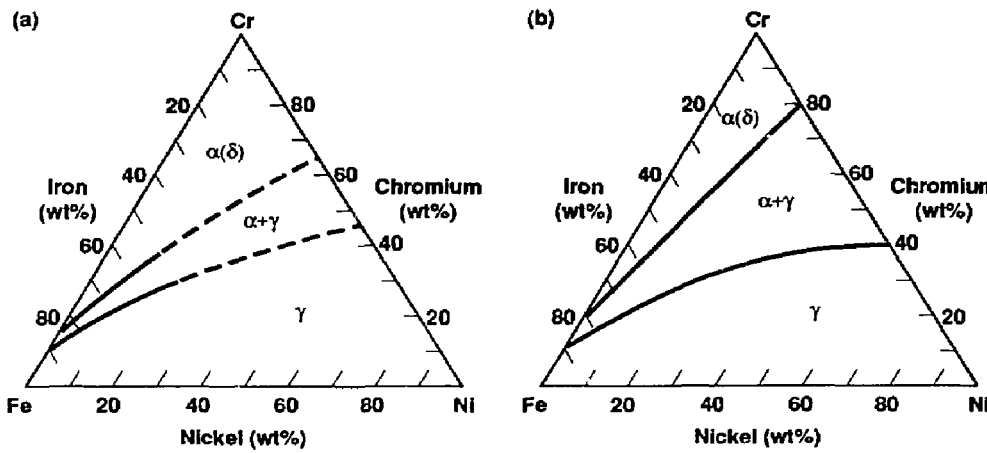


Figure 3. Iron-chromium-nickel ternary equilibrium phase diagram. (a) Phases in the temperature range of maximum austenite formation (900 to 1300°C) [6]. (b) Phases at 1100°C [7].

Figure 3(a) shows a typical phase diagram in the temperature range for maximum austenite formation (900°C < T < 1300°C) [6]. Figure 3(b) shows similar data from another author indicating the phases present at 1100°C [7]. These diagrams differ because of temperature, alloy purity, and differences in experimental technique. However, at the high iron concentrations the diagrams are very similar. The ranges of composition for Types 304 and 316 stainless steels fall almost completely within the austenite (γ) field. Higher-temperature annealing would cause most of the alloy composition for Types 304 and 316 stainless steels to fall within the two-phase region [austenite (γ) and ferrite (α)], as shown in Fig. 4. This figure shows an iron-chromium-nickel ternary equilibrium phase diagram that identifies the phases present at slightly below the solidus temperature.

The metastability of the austenitic phase is dependent upon the thermomechanical history of the material. Figure 5 is an iron-chromium-nickel ternary diagram showing regions of stability and metastability. (Note that in Fig. 5(a) there is 0.1 wt% carbon.) This figure does not represent equilibrium conditions, as those would be expected for infinitely long cooling times. Figure 5(a) shows the stable and metastable phases present at room temperature after rapid cooling from the temperature range that produces maximum austenite content [6]. Note the large region of metastable austenite ($A_M$) and the regions of martensite and ferrite structure. This metastable austenite is present in Types 304L and 316L stainless steels and not in Alloy 825. The structure of alloys quenched from a temperature of 1100°C is shown in Fig. 5(b) [8]. The stable austenite region is slightly reduced, with an increase in the regions where austenite may transform to martensite upon cold working.

The ranges of austenite stability presented in the two diagrams in Fig. 5 differ because of compositional variation. Commercial alloys usually retain the austenitic microstructure at room temperature, as indicated in Fig. 5(a). More recent work on alloys with lower carbon content and more detailed microchemical analysis reveal transformation of austenite at temperatures as low as room temperature, as indicated in Fig. 5(b). At least part of the variation in austenite stability

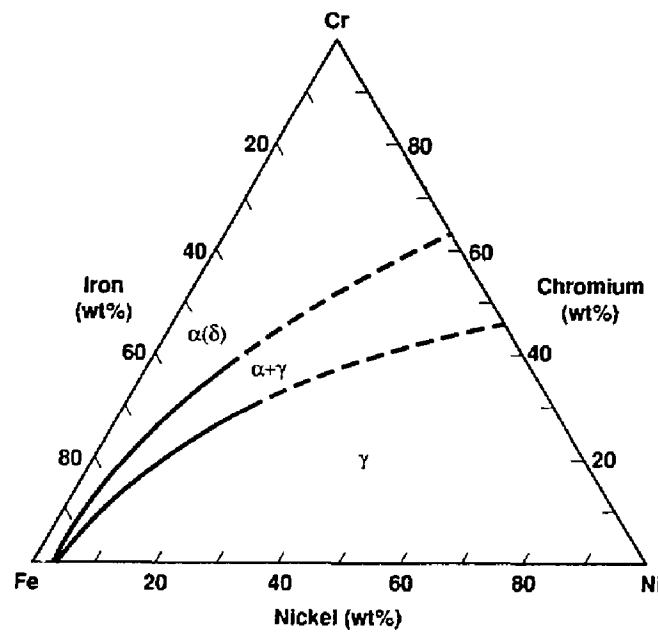


**Figure 4. Iron-chromium-nickel ternary equilibrium phase diagram at a temperature just below the solidus. Solidus temperatures are about 1400 to 1450°C [8].**

$A_M$ = metastable austenite
$A_S$ = stable austenite
F = ferrite (from austenite)
$F_D$ = delta (high-temperature) ferrite
M = acicular (martensitic) structure
C = carbide
P = pearlite

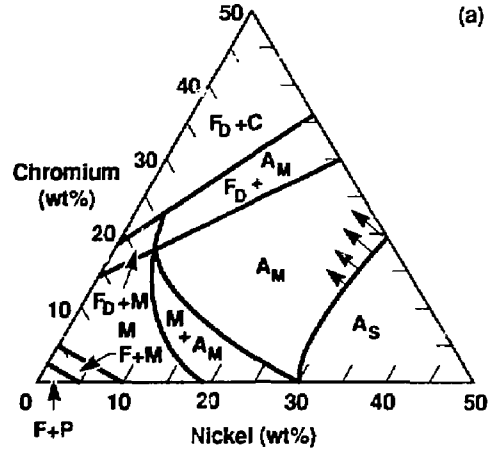


$\alpha_m$ = ferrite formed by massive $\gamma \rightarrow \alpha$ transformation
$M_L$ = martensite in which units are small laths
$M_\rho$ = martensite in which units are large plates
$M_\varepsilon$ = hexagonal close-packed martensite
$\gamma_u$ = unstable austenite (may transform if cold-worked)
$\gamma_S$ = stable austenite

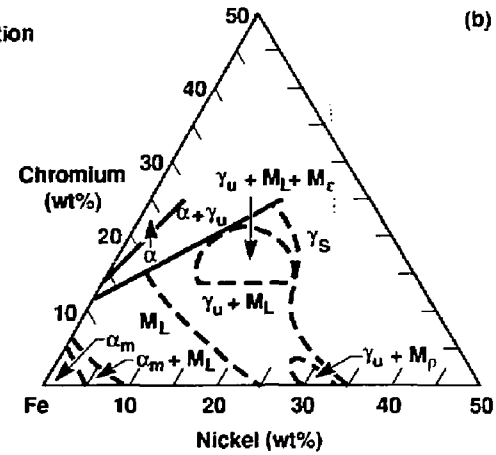


**Figure 5. Iron-chromium-nickel ternary metastable phase diagram. (a) Phases after quenching from temperature range of maximum austenite formation. Carbon content is 0.1 wt% [6]. (b) Phases after quenching from 1100°C [8].**

is due to lower carbon content. Low-temperature conversion to the different transformation products shown will be discussed in later sections.

## 2.3 Chromium and Nickel Equivalents

Thus far, the austenitic alloys have been described primarily in terms of the iron-chromium-nickel ternary diagram. These alloys actually contain a number of minor alloying elements, as indicated in Table 1. It would be extremely difficult to visualize a multidimensional phase diagram to represent this large number of constituents. However, the constitution of austenitic alloys can be estimated using the concept of nickel and chromium equivalents. The alloying elements that have been shown to stabilize the austenite-phase field are assigned a corresponding nickel equivalent. Similarly, the ferrite-

stabilizing elements are assigned a corresponding chromium equivalent. Equations defining the nickel and chromium equivalents for common austenitic alloy constituents have long been employed to predict what phases will be present in iron-chromium-nickel alloy systems [9–15]. Recent work by Harries [10] yields the following equivalent equations. The nickel equivalent is given by:

$$\text{Ni (equiv.)} = \text{Ni\%} + \text{Co\%} + 0.5\,\text{Mn\%} + 30\,\text{C\%} + 0.3\,\text{Cu\%} + 25\,\text{N\%} \quad (1)$$

The chromium equivalent is given by:

$$\text{Cr (equiv.)} = \text{Cr\%} + 2\,\text{Si\%} + 1.5\,\text{Mo\%} + 5\,\text{V\%} + 5.5\,\text{Al\%} + 1.75\,\text{Nb\%} + 1.5\,\text{Ti\%} + 0.75\,\text{W\%} \quad (2)$$

Use of these equations permits the construction of equivalent ternary phase diagrams that can be employed to predict the phases present in a system under certain conditions. These equivalents will be employed in later sections of this report, which address the precipitation of other phases ($\chi$, $\sigma$, and $\eta$) from austenite over long time periods.

Using Eqs. (1) and (2), it is possible to determine nickel and chromium equivalents for each candidate alloy. The results of these calculations are listed in Table 2. These data may now be plotted on the iron-chromium-nickel system ternary diagram. This has been done in Fig. 6 for a temperature of 650°C. Note that Types 304L and 316L stainless steels are plotted as points in the $\gamma$-phase field near the $\alpha + \gamma$ phase region. The nickel and chromium equivalents for Alloy 825 indicate that this alloy is located well within the $\gamma$-phase field at this temperature. It should be noted that these alloys exist over a range of compositions, as indicated in Table 1. The accuracy of the calculations of chromium and nickel equivalents is about ±4%. This implies that there are compositions of Types 304L and 316L stainless steels that would fall into the $\gamma + \sigma$ or $\gamma + \alpha$ phase field at 650°C. (The presence of two phases has adverse effects on the mechanical and corrosion properties of these alloys.)

There has been significant utilization of nickel and chromium equivalents in welding technology. These equations have been primarily employed to determine the effects of additions of alloying elements on ferrite formation in weld filler material. This work has been summarized by Campbell [16]. There has been no coordinated effort to refine the equivalents technique to wrought or cast alloys. Hence, the phase diagrams constructed from equivalents data should be viewed as general and approximate indications of trends that might be expected.

## 2.4 Martensite Transformations

Transformation in the iron-chromium-nickel system is very complicated and has been the subject of many investigations [e.g., 17–22]. It has long been known that the low-alloy fcc austenites ($\gamma$) transform to bcc martensite ($\alpha'$) at or below room temperature. This is a shear transformation that is usually driven by the stacking-fault energy of the alloy. As noted in Fig. 5(b), there are two types of martensite formed, $\alpha'$-bcc [$M_L$ and $M_\rho$ in Fig. 5(b)] and $\varepsilon$-hcp [$M_\varepsilon$ in Fig. 5(b)]. Considerable effort has been directed toward identification and definition of these types of martensite with respect to morphology and mechanisms of formation. The occurrence of the different types of martensite is composition-related, as shown in Fig. 5(b).

The martensite phase that has generated the greatest interest is the hcp phase, $\varepsilon$ martensite. The $\varepsilon$ martensite is commonly found in conjunction with $\alpha'$ martensite. Hence, researchers have attempted to determine whether $\varepsilon$ martensite is an intermediate phase in the formation of $\alpha'$ martensite or a separate constituent that could form as a result of the strain generated by the $\gamma$ to $\alpha'$ transformation. Since $\varepsilon$ martensite is

**Table 2. Nickel and chromium equivalents (wt%) for the austenitic candidate alloys, calculated using equations from Harries [10].**

| | 304L stainless steel | 316L stainless steel | Alloy 825 |
|---|---|---|---|
| **Nickel equivalent** | 14.4 | 16.4 | 44.7 |
| **Chromium equivalent** | 21.0 | 22.8 | 25.0 |

nonmagnetic and is difficult to define clearly in an optical microscope, x-ray diffraction techniques and transmission electron microscopy with energy-dispersive x-ray analysis are required for its identification. Dash and Otte [22] suggest instances of independent formation of the two phases. Figure 7 represents a summary of the hypothetical paths for the formation of α′ martensite from γ austenite. Work by Cina [23], Reed [24], and Breedis and Robertson [25] indicate that the hcp ε structure is an intermediate phase in the formation of α′ martensite. Hence, it appears that ε martensite is usually involved in some aspect of the α′ transformation process.

Austenite-to-martensite transformation, which is influenced by alloy composition, temperature, strain, and strain-rate effects, has been defined by the temperature at which α′ martensite forms upon cooling ($M_s$) and the temperature at which α′ martensite will be formed under deformation conditions ($M_d$). Comparison of the relative values of $M_s$ and $M_d$ for Types 304L and 316L stainless steels indicates that Type 304L is more susceptible to martensite formation than Type 316L. The $M_s$ temperature for Type 304L is approximately 50 K higher than for Type 316L. There has been no documentation of martensite formation in Alloy 825. This is to be expected, since Alloy 825 is located in the austenite-stable region far from the austenite-ferrite phase boundary (Fig. 6).

The formation of martensite can have an adverse affect on the mechanical properties of the alloy. The martensite phase is considerably harder and more brittle than the austenite phase. This transformation is not desirable in the materials that will be employed in the metal barrier for the NWMP. A determination of the maximum allowable degree of martensite formation would be required if Type 304L or 316L stainless steel were

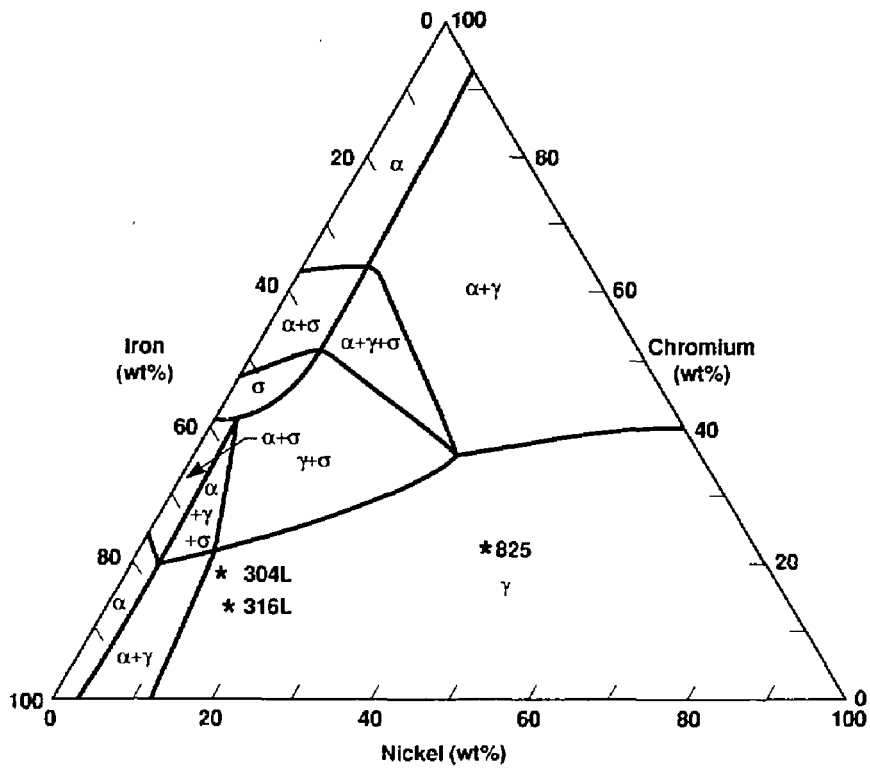


**Figure 6. Iron-chromium-nickel equilibrium phase diagram at 650°C [3]. Note the location of Alloys 304L, 316L, and 825, plotted using nickel and chromium equivalent values.**

to be used. The martensitic transformation would not be a problem if Alloy 825 were to be employed as the container material.

## 2.5 Carbide Formation

The ubiquitous carbide in iron-based austenitic alloys is $M_{23}C_6$. This carbide is formed in the absence of any strong carbide-forming elements. If strong carbide-forming elements are present, $M_{23}C_6$ is usually formed in equilibrium with these carbides. The low-carbon austenitic alloys proposed for use as container materials will be less susceptible to carbide precipitation than will typical commercial alloys. However, there is still the possibility of carbide precipitation. This precipitation at grain boundaries can result in a phenomenon known as sensitization. This phenomenon is actually the result of concomitant chromium depletion near the carbide. A sensitized material is more susceptible to intergranular stress corrosion cracking (IGSCC) than an unsensitized one. IGSCC often causes catastrophic failure and is discussed further in Vol. 3.

A significant body of data exists in the literature on the nucleation and growth of carbide precipitates in austenitic alloys [26–30]. Cihal [26] and Stickler and Vinckier [27] completed studies on the precipitation of $M_{23}C_6$ carbides in Types 304 and 304L stainless steels. These studies utilized optical microscopy, and intergranular carbide formation was detected by $H_2SO_4$-$Cu_2SO_4$ tests. The results of these investigations are presented in Figs. 8 and 9. Figure 8 presents two time-temperature precipitation (TTP) diagrams for Type 304 stainless steel. Figure 8(a) shows the precipitation of $M_{23}C_6$ carbides as a function of temperature and location of formation as determined by Cihal. The results of Stickler and Vinckier, which are presented in Fig. 8(b), indicate initial $M_{23}C_6$ carbide precipitation at austenite-ferrite interfaces. Carbides next form on grain boundaries, followed by precipitation on noncoherent and coherent twin boundaries, respectively. These precipitation curves do not agree exactly. This is to be expected, since the curves were derived from x-ray and electron microscopy data from two alloys that were not identical. The precipitation of $M_{23}C_6$ carbides in

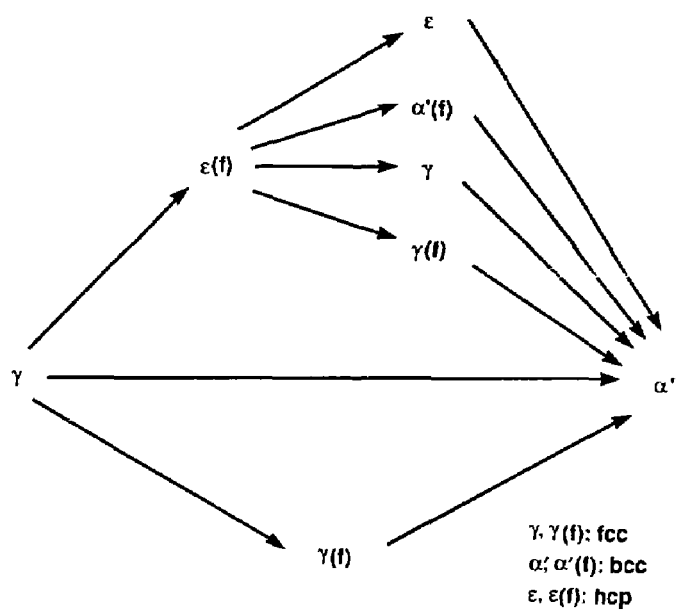


Figure 7. Possible paths for the formation of α′ martensite from γ austenite. The symbol (f) indicates the faulted structure of the phase [22].

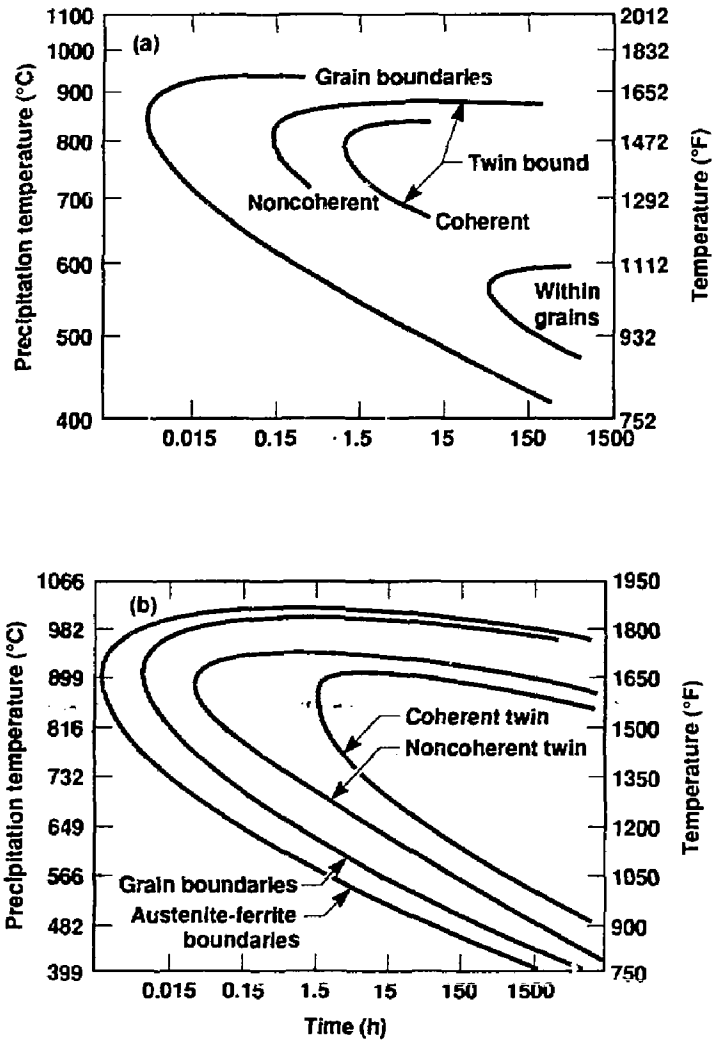


Figure 8. Precipitation kinetics of $M_{23}C_6$ carbides in Type 304 stainless steels. (a) Alloy containing 0.05 wt% C, originally quenched from 1250°C [26]. (b) Alloy containing 0.038 wt% C, originally quenched from 1260°C [27].

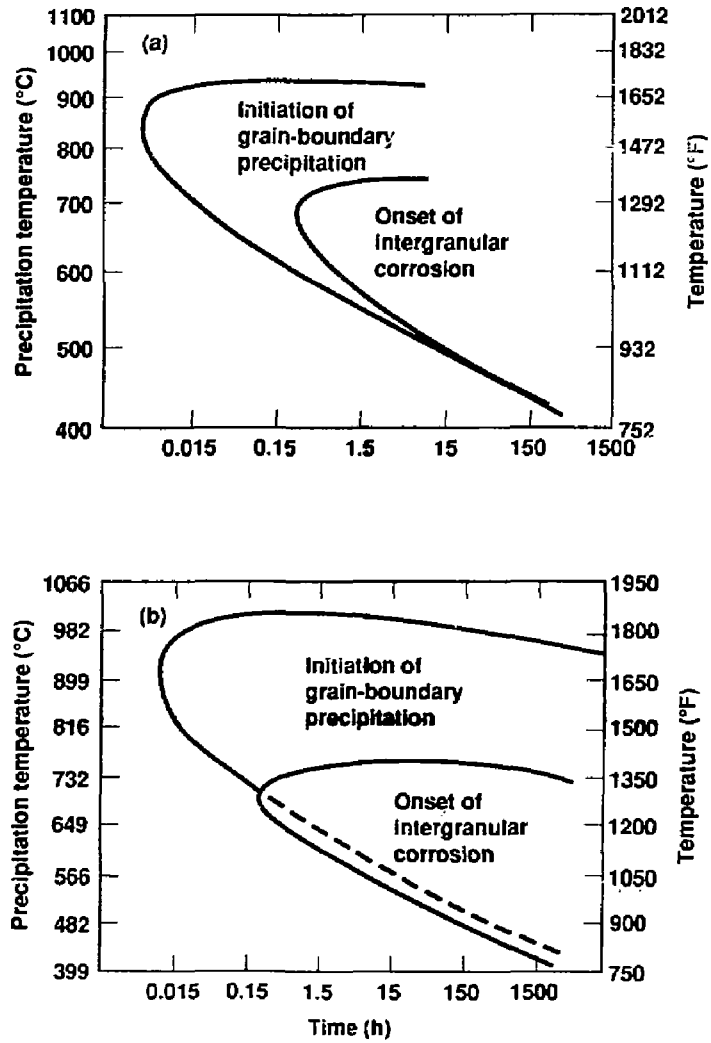


**Figure 9. Effect of $M_{23}C_6$ carbide precipitation on intergranular corrosion in Type 304 stainless steels. (a) Alloy containing 0.05 wt% C, originally quenched from 1250°C [26]. (b) Alloy containing 0.038 wt% C, originally quenched from 1260°C [27].**

Type 316 stainless steel is similar to the results presented in Fig. 8(b). The only difference is that the times for precipitation are slightly shorter [28], but sensitization occurs at longer times.

Carbide precipitation at grain boundaries can lead to local depletion of chromium (sensitization), resulting in increased susceptibility to intergranular corrosion. Cihal [26] and Stickler and Vinckier [27] measured the onset of intergranular corrosion as a function of precipitation time and temperature. The results of these tests are summarized in Fig. 9. Both Cihal [Fig. 9(a)] and Stickler and Vinckier [Fig. 9(b)] observed the earliest onset of intergranular corrosion after treatment at a temperature of about 650°C. The observation of intergranular corrosion lags behind the initiation of precipitation. This is most likely due to the fact that corrosion resistance is

not significantly diminished until a significant depletion in chromium at the grain boundary has been attained.

Carbide precipitation studies have also been completed on Types 316 and 316L stainless steels. Weiss and Stickler [28] determined the effect of annealing temperature on the carbide precipitation kinetics of Type 316L, as shown in Fig. 10. Note that for the specimen with the higher annealing temperature (1260°C vs 1090°C), the precipitation of $M_{23}C_6$ carbides began at shorter times.

Weiss and Stickler [28] also made a comparison of the precipitation kinetics of $M_{23}C_6$ carbides in Types 316 and 316L stainless steels, as shown in Fig. 11. The reduction in carbon content delays the onset of carbide precipitation at higher temperatures (>700°C). This allows for short-term, high-temperature excursions, such as welding, with no carbide precipitation. At lower temperatures and longer time periods, there is virtually no difference between the precipitation kinetics of Types 316 and 316L. This behavior may prove to be a significant factor in the degradation of the mechanical and corrosion properties of Type 316L in a repository environment.

If enough carbide precipitation occurs, the depletion of chromium and carbon in the matrix may result in transformation of the previously stable austenite to another phase. This phenomenon is indicated in Fig. 12 for Type 304 stainless steel [27]. Significant $M_{23}C_6$ carbide precipitation resulted in the transformation of the stable austenite to martensite upon cooling to 77 K. This occurred only after relatively long time periods at elevated temperatures. However, it is informative to note that the possibility of this phenomenon exists and may be possible in the long time periods (300–1000 yr) required for containment in the repository environment.

The long-term, low-temperature precipitation of $M_{23}C_6$ carbides in Types 304L and 316L stainless steels may have a significant impact on the mechanical and corrosion properties of these materials. The data presented in Figs. 8 through 12 indicate the onset of grain-boundary precipitation of $M_{23}C_6$ carbides at lower temperatures as time increases ($t > 1500$ hr). This precipitation is also greatly affected by the formation of intermetallic phases, as presented in the following section.

## 2.6 Intermetallic Phases

Alloy systems based on the transition metals iron and nickel, which also contain titanium, vanadium, or chromium, can form a number of intermetallic phases. The austenitic stainless

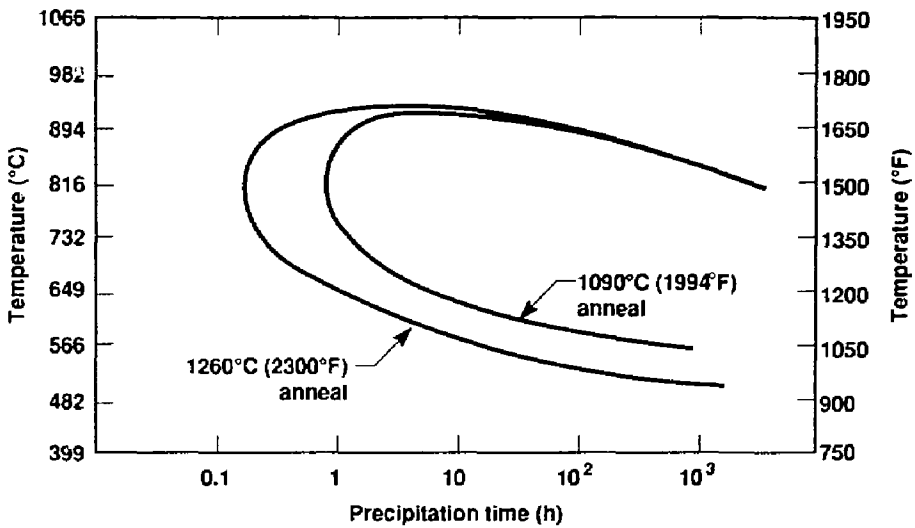


Figure 10. Effect of annealing temperature on subsequent $M_{23}C_6$ carbide precipitation kinetics in Type 316L stainless steel [28].

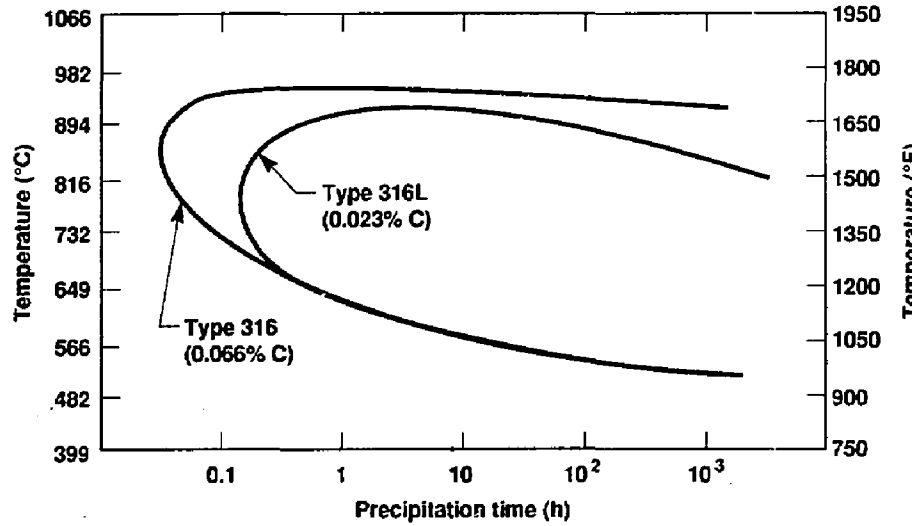


Figure 11. Comparison of precipitation kinetics in Types 316 and 316L stainless steels as determined by transmission electron microscopy techniques [28].

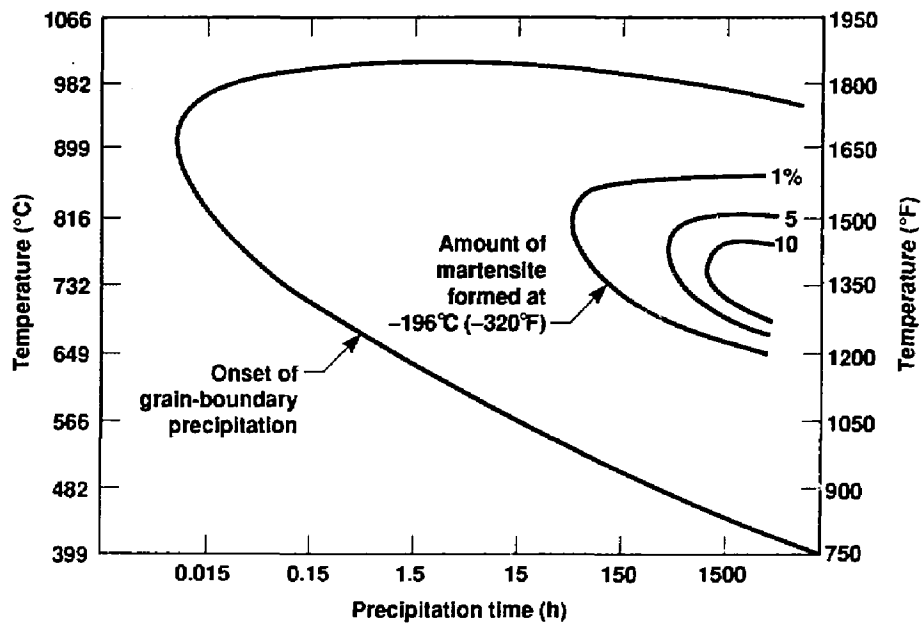


Figure 12. Effect of $M_{23}C_6$ precipitation on austenite stability in Type 304 stainless steel [27].

steels can form sigma (σ), chi (χ), and Laves (η) phases, which are thermodynamically stable. The compositions of these phases can adhere strictly to the prescribed stoichiometric ratios, or the phases can exist over a range of compositions. The σ phase, which has a complex tetragonal structure, can range in composition from $B_4A$ to $A_4B$, with A being nickel and iron, and B being chromium and molybdenum. The χ phase has a bcc-αMn structure with the formula $(FeNi)_{36}Cr_{12}Mo_{10}$ [28], while the Laves phase has a hexagonal structure with the formula $Fe_2Mo$ [31]. The occurrence of these phases is dependent on the electron/atom ratio, atomic size, and atomic compressibility. The conditions under which these phases form are quite complex. This complexity is compounded by the fact that these phases usually do not form independently. Hence, competition for a particular constituent atom can become an important factor. These phases generally precipitate over the temperature range $600°C < T < 1150°C$.

The σ phase has been extensively studied because of its occurrence in alloys used at elevated temperatures. It is a hard, brittle, nonmagnetic phase in stainless steel that was first noted by Bain and Griffiths [32]. In Type 304 stainless steel, σ formation is promoted by the presence of silicon. Silicon appears to broaden the composition range over which the σ phase is stable. The addition of molybdenum, as in Type 316 stainless steel, tends to further broaden the σ phase range of stability. Phase-equilibrium diagrams for a 70% iron alloy containing molybdenum, nickel, and chromium were determined by Bechtoldt and Vacher [31] and are presented in Fig. 13. Note that in the region near the composition of Type 316L stainless steel (16–18 Cr, 10–14 Ni, 2–3 Mo), the equilibrium phases that are present change from $(\alpha + \gamma)$ at 1204°C to $(\sigma + \gamma + \chi + \eta)$ at 815°C. With increasing molybdenum content, the σ and χ phases tend to change to χ and Laves phases.

The formation of σ phase in austenitic alloys leads to a reduction in fracture toughness. This reduction in toughness is most pronounced at ambient temperatures, as shown in Fig. 14. This figure indicates a dramatic decrease in fracture toughness with increasing σ content in high-nickel, high-chromium austenitic alloys. Although the effect will not be as pronounced in Type 316L stainless steel, the formation of even a small amount of σ phase can have a significant impact on the mechanical properties. This effect is primarily a problem at temperatures below about 600°C [33]. Intergranular corrosion of alloys containing σ phase is also a problem in an oxidizing environment [34]. Sigma phase is not resistant to strong oxidizing media such as hot concentrated nitric acid. This lack of resistance leads to intergranular attack when the σ phase is distributed along grain boundaries.

## 2.7 Precipitation Studies

The most useful method of determining the stability of a particular alloy is to complete a precipitation study. TTP diagrams indicate the conditions required for precipitation of equilibrium phases to be formed. Precipitation in Type 304 stainless steel has been adequately described in Sec. 2.5 above, since $M_{23}C_6$ is the predominant precipitate phase. TTP diagrams for Type 316 stainless steel are presented in Figs. 15 and 16 [28, 30]. Figure 15 shows the TTP diagram for Type 316 stainless steel and the variation in precipitate distribution as a function of time for a Type 316 stainless steel aged at 816°C for up to 10,000 hr. Note the increase in $M_{23}C_6$ concentration beginning almost immediately. The χ phase begins to precipitate at about 150 hr, while the σ and Laves phases do not begin to precipitate until about 500 and 1000 hr, respectively.

Similar plots for Type 316L stainless steel are presented in Fig. 16. This figure also indicates the effects of different annealing temperatures and cold-work conditions on precipitate formation. Note the decrease in the amount of $M_{23}C_6$ phase at increasing times. The authors [28] believe that the carbides dissolve after reaching a maximum. Also note the acceleration of the precipitation of $M_{23}C_6$ and σ due to the effects of cold work.

Precipitate formation in Types 304L and 316L stainless steels could have a significant impact on the mechanical properties and corrosion resistance of these materials. The studies outlined here indicate that these alloys can undergo significant microstructural evolution at moderate temperature ($T < 650°C$) over relatively short times ($t < 1000$ hr). Repository temperature, though considerably lower ($T < 250°C$) could promote precipitation in the time period of interest for container retrieval ($t < 450{,}000$ hr). Studies of long-term, low-temperature phase stability or computer modeling of the diffusion of precipitate constituents may be required to determine the potential use of Types 304L and 316L stainless steels as container materials.

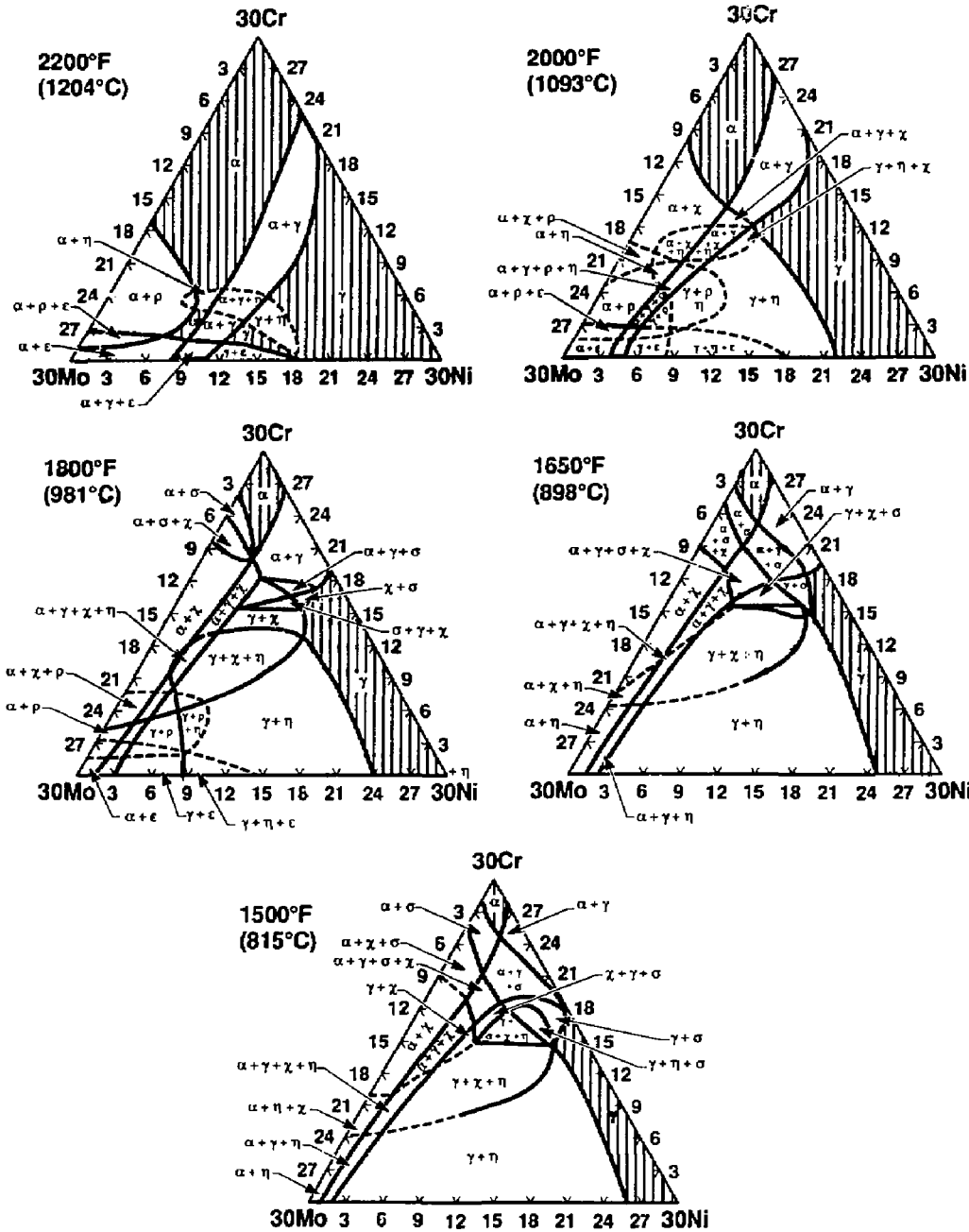


Figure 13. Phase equilibrium for high-purity iron-chromium-nickel alloys containing 70% iron [31].

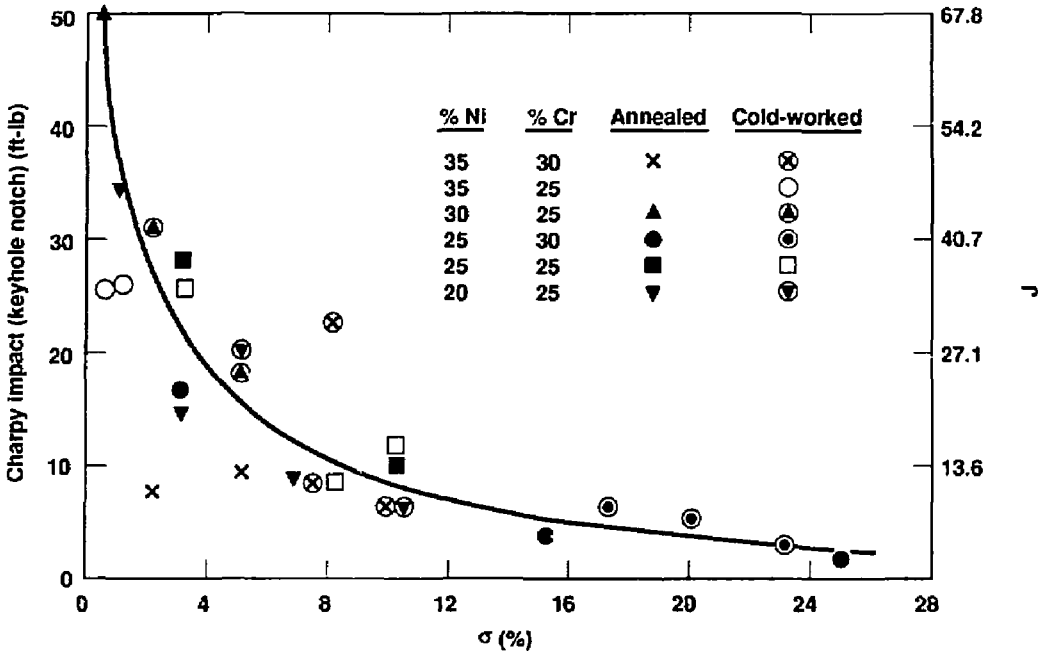


**Figure 14. Effect of σ phase formation on room temperature impact strength of iron-chromium-nickel alloys [33].**

## 2.8 Alloy 825

A survey of the technical literature with respect to phase stability in Alloy 825 provided very little data or information. Few studies on phase stability in Alloy 825 were identified Brown and Kirchner [35] completed a survey of the corrosion of high-alloy weldments that included a brief description of the resistance of Alloy 825 to sensitization. Brown [36] evaluated a number of Alloy 825 samples with various heat treatments in corrosive environments and noted a wide variation in resistance to sensitization. Copson et al. [37] reported inconclusive evidence for the presence of σ phase in Alloy 825. Raymond [38] studied the sensitization of Alloy 825 due to $M_{23}C_6$ precipitation at grain boundaries. These studies constitute the limited information identified in this literature survey. A review of the superalloy literature was completed to provide general background with respect to phase stability in these systems [39–44]. No significant intermetallic-phase formation was identified in Alloy 825.

Alloy 825 is an austenite-stable material throughout the entire temperature range from solidus temperature to room temperature. It does not undergo transformation to martensite or ferrite, as do Types 304 and 316 stainless steels. Figure 17 indicates the difference in phase stability between Alloy 825 and the stainless steels. Types 304 and 316 stainless steels, which contain approximately 70% iron, have α and γ in equilibrium at low temperatures. Alloy 825, which contains about 30% iron and 40% nickel, has a stable γ phase throughout the entire temperature range, as indicated by the left side of Fig. 17. The transition to full austenite stability occurs at an iron content between 60 and 70% for alloys of higher nickel content.

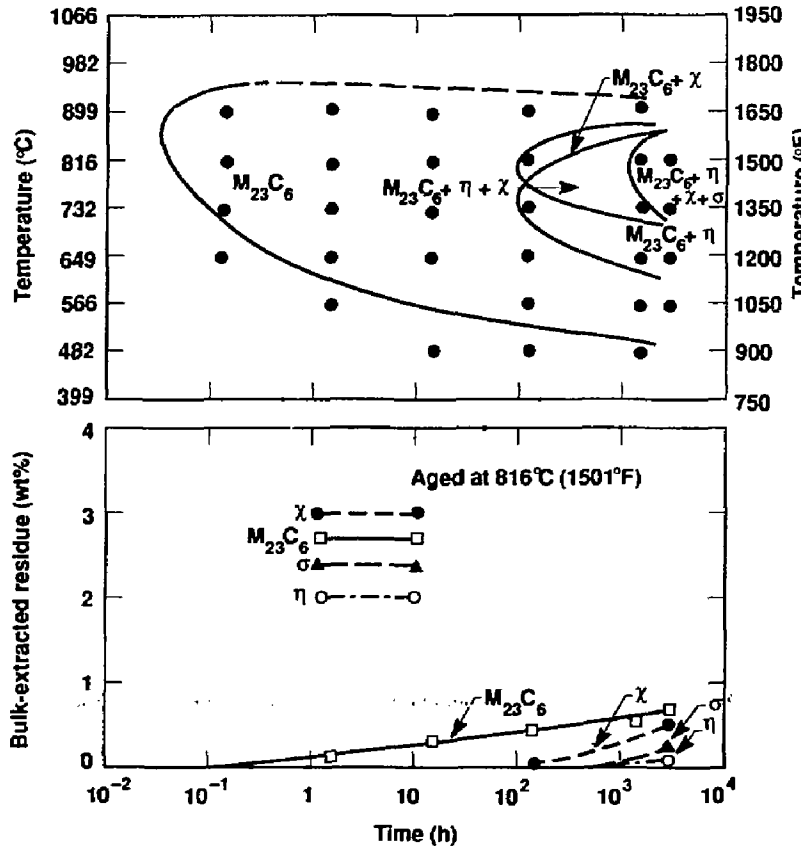


**Figure 15. Time-temperature-precipitation diagram for Type 316 stainless steel initially annealed at 1260°C [28].**

Precipitation of the $M_{23}C_6$ carbide was noted in Alloy 825 by Raymond [38] after various anneal times. Raymond completed transmission electron microscopy studies of Alloy 825 using extraction-replica techniques and jet-machined thinning processes. The extraction-replica technique permits the determination of the chemical composition of the carbide precipitates by energy-dispersive x-ray analysis (EDX). Using this technique, Raymond found that carbide composition did not correlate with susceptibility to sensitization. The $M_{23}C_6$ carbide in Alloy 825 may have significant quantities of titanium in addition to chromium, depending on the specimen's annealing history.

A stabilization treatment is required in order to make Alloy 825 resistant to sensitization [38]. According to Raymond, carbon solubility is limited in Alloy 825, being at most 0.01 wt% for temperatures less than 970°C. Typically, Alloy 825 has about 0.0 wt% carbon; therefore, carbide precipitation will occur under certain conditions. Titanium is a strong carbide former, and typically about 1.0 wt% is added to this alloy. Raymond found that the titanium can bind only about 0.01 wt% of the carbon as TiC. Stabilization against sensitization is obtained by precipitating the active carbon as $M_{23}C_6$ carbide and by annealing further to diffuse chromium back into the

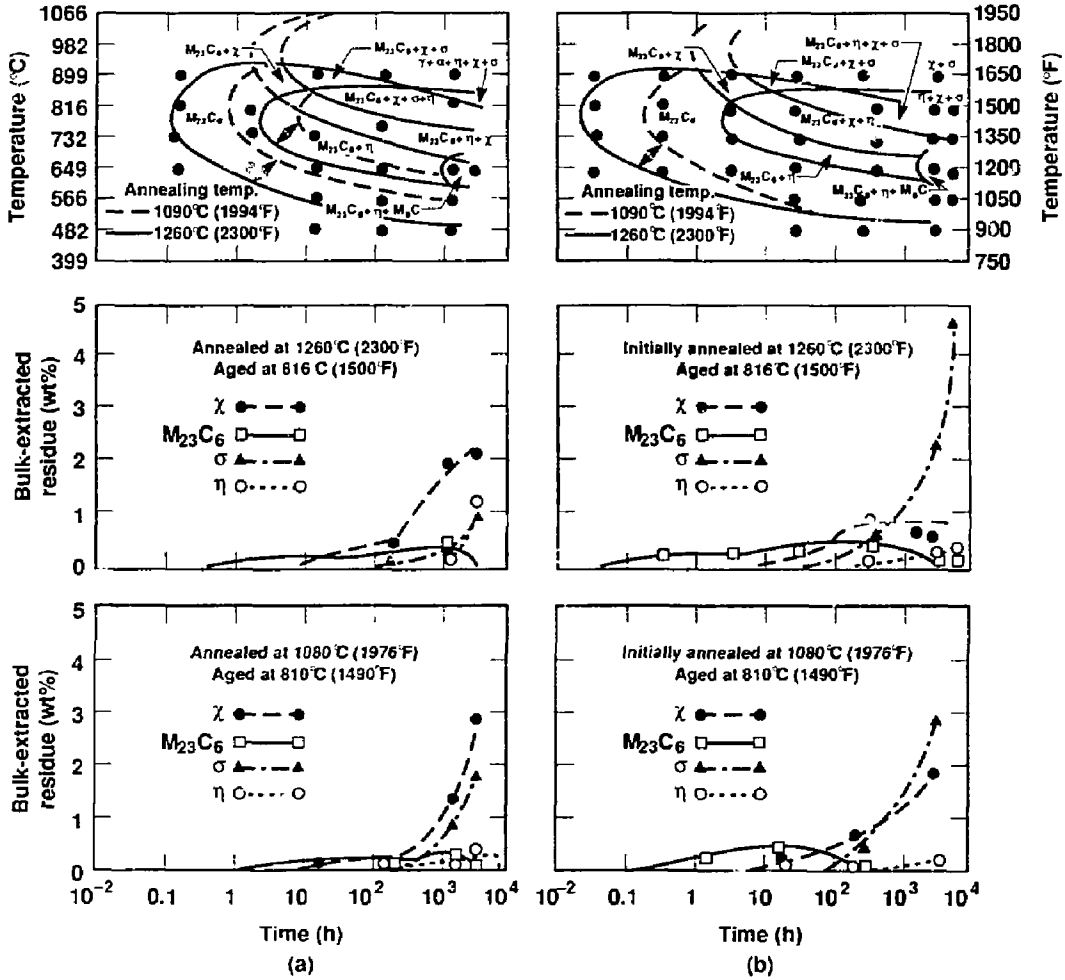


Figure 16. Time-temperature-precipitation diagram for Type 316L stainless steel. (a) Annealed. (b) Cold-worked 20% [28, 30].

depleted regions. Typically, annealing for 1 hr in the temperature range of 925 to 970°C is satisfactory for achieving stabilization of this alloy.

The effect of the stabilization treatment is illustrated in Fig. 18 [38]. Figure 18(a) is a time-temperature-sensitization diagram for Alloy 825 annealed at 1090°C for 1 hr prior to sensitization. (The solution anneal at 1090°C dissolves the carbides and allows reprecipitation upon annealing at lower temperatures.) Significant sensitization was found in the temperature region around 760°C. If Alloy 825 is annealed for 1 hr at 940°C prior to sensitization treatment, its resistance to sensitization is significantly enhanced, as shown in its time-temperature-sensitization diagram [Fig. 18(b)].

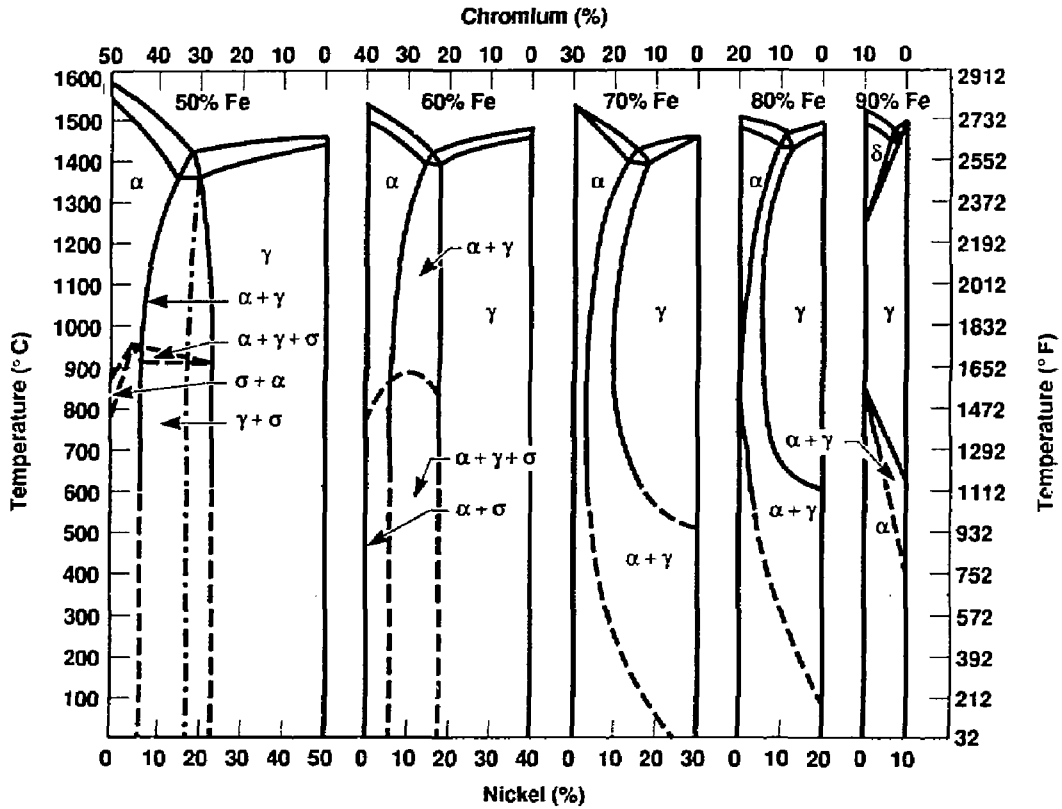


**Figure 17. Cross sections of iron-chromium-nickel ternary phase diagram [7]. The dashed lines indicate that the phase transformations do not occur under practical conditions.**

The precipitation of other intermetallic phases in Alloy 825, such as σ, χ, or η, has not been noted in the literature. Brown [36] and Copson et al. [37] have suggested the presence of submicroscopic σ phase in order to explain the alloy's susceptibility to sensitization following various annealing sequences. Brown [36] found that stabilizing anneals near 935°C for 1 hr, after a solution anneal at 1090°C for 1 hr, were not able to prevent the specimens from becoming sensitized at lower temperatures. In his studies, Brown used boiling 65% nitric acid to test for sensitization. This test has been previously shown to be sensitive to σ formation in Type 316L stainless steel. Since both Alloy 825 and Type 316 stainless steel contain molybdenum, which promotes σ formation in stainless steels, it was suggested that σ formation may account for the experimental observation just discussed. It should be mentioned, though, that increasing the nickel content of an austenitic alloy has been shown to reduce the tendency to σ formation [2].

Austenite stability, the capability to be stabilized against sensitization, and the lack of significant intermetallic-phase formation suggest that Alloy 825 would provide the most stable material of the austenitic candidates discussed in this volume.

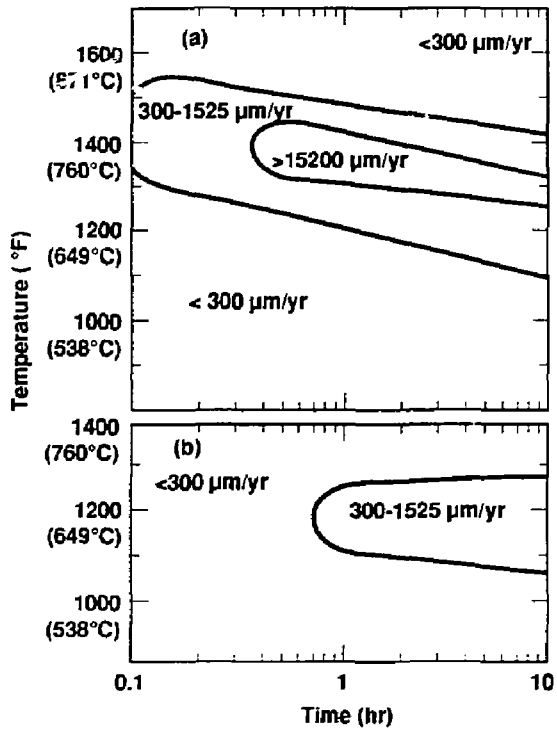


**Figure 18. (a) Time-temperature-sensitization diagram for Alloy 825 annealed at 1093°C for 1 hr prior to sensitization treatment [38]. (b) Time-temperature-sensitization diagram for Alloy 825 annealed at 940°C for 1 hr prior to sensitization treatment [38].**

## 3. Summary of the Survey of Austenitic Candidate Alloys

A review of the technical literature with respect to phase stability of the candidate austenitic materials Types 304L and 316L stainless steels and Alloy 825 has been completed. Significant data dealing with phase stability were noted for the stainless steel alloys. Types 304L and 316L stainless steels were identified as metastable materials under repository-relevant conditions. Metastability is defined as nonequilibrium phase formation due to kinetic limitations. In Types 304L and 316L stainless steels, the diffusion processes that permit precipitation are severely limited at low temperatures ($T < 600°C$).

Carbide precipitation was identified in all of the austenitic candidate alloys. The precipitation of $M_{23}C_6$ carbides was predominant in Types 304L and 316L stainless steels. Intermetallic-phase formation was noted in Type 316L stainless steel at relatively long times. These intermetallic phases include σ, χ, and Laves phases. Sigma-phase formation was shown to significantly reduce the impact strength of austenitic stainless steels because of its hard, brittle microstructure. No intermetallic-phase formation was documented for Alloy 825.

Very few data on phase stability were identified for Alloy 825. This alloy is austenite-stable from its solidus temperature to room temperature. Limited data were found that dealt with carbide precipitation. Titanium can be precipitated as TiC; this carbide binds about 0.01 wt% carbon in the material. The mode of precipitation

of the $M_{23}C_6$ carbides greatly affects whether Alloy 825 can be sensitized. A stabilization anneal at 970 to 925°C for 1 hr was found to precipitate $M_{23}C_6$ carbides but also cause chromium diffusion back into the previously chromium-depleted regions. This stabilization treatment enhances Alloy 825's resistance to sensitization. Speculation about the possibility of "submicroscopic" σ-phase precipitation in Alloy 825 was noted.

## 4. Ranking of the Austenitic Candidate Alloys

Considering the effect of phase stability only, the following ranking of the austenitic candidate materials is proposed:

1. Alloy 825
2. Type 316L stainless steel
3. Type 304L stainless steel

This order is based on the fact that Alloy 825 is a stable austenite at all temperatures and that it can be stabilized against sensitization with proper heat treatment.

Type 316L stainless steel is susceptible to intermetallic-phase formation, including the formation of the σ phase. Sigma-phase formation can result in significant degradation of the mechanical properties of the alloy. Type 316L stainless steel is also affected by $M_{23}C_6$ carbide precipitation, which could deplete chromium near the precipitates and promote grain-boundary attack.

Type 304L stainless steel also exhibits significant $M_{23}C_6$ carbide precipitation, which could result in grain-boundary attack. This alloy is also more prone to martensite formation than is Type 316L stainless steel.

## 5. Copper-Based Candidate Alloys

The copper-based candidate alloys that have been selected for consideration by the Nuclear Waste Management Program (NWMP) are CDA 102, CDA 613, and CDA 715. Representative compositions of these materials are given in Table 3 [45]. CDA 102 is oxygen-free, high-conductivity (OFHC) copper. Both CDA 613 and CDA 715 are solution-hardened materials. The addition of alloying elements improves the mechanical and corrosion properties in some

Table 3. Composition of copper-based candidate alloys (wt%) [45].

| Alloy | Cu | Ni | Al | Mn | Sn | Fe | Zn | Other |
|---|---|---|---|---|---|---|---|---|
| CDA 102 | 99.95 | — | — | — | — | — | <0.001 | Pb < 0.001 |
| | | | | | | | | Cd < 0.001 |
| | | | | | | | | S < 0.0018 |
| | | | | | | | | Hg < 0.0001 |
| | | | | | | | | P < 0.003 |
| CDA 613 | 90.82 | 0.05 | 6.75 | 0.16 | 0.20 | 2.46 | 0.01 | Pb < 0.01 |
| | | | | | | | | Co < 0.01 |
| CDA 715 | 69.18 | 29.60 | — | 0.51 | — | 0.53 | 0.07 | Pb, 0.01 |
| | | | | | | | | P, 0.002 |
| | | | | | | | | C, 0.04 |
| | | | | | | | | S, 0.01 |

environments. The phase stability of each copper alloy is addressed separately in the following sections.

## 5.1 CDA 102

CDA 102 is essentially pure copper (99.95 wt%) with a very small impurity content (see Table 3). Copper is a single-phased, face-centered cubic (fcc) metal at all temperatures [46]; therefore phase stability is not a concern. What is of concern, though, is the reaction of copper with oxygen to form copper oxide phases. The formation of oxide will be enhanced under repository conditions because of the presence of aerated water [47] and because of radiolysis. Oxides form at very small oxygen concentrations in the repository because oxygen solubility in copper is negligible at repository temperatures [48, 49]. The oxidation and corrosion of copper are discussed elsewhere [1].

In addition, copper oxides can be formed during welding [1]. These oxides are not soluble in copper and therefore populate the grain boundaries, where they can be reduced by hydrogen. This reduction causes the formation of trapped gas, which can have an especially deleterious effect on weld integrity [1].

Deoxidants can be added to the pure copper to alleviate the problem of copper oxide formation in the weld region [46]. The deoxidants form more stable oxides than copper does, and the deoxidant oxides remain in solution upon cooling. Phosphorus is one of the more common deoxidants, with several commercial alloys available. These range from CDA 103, whose phosphorus content is extra low (0.003 wt%), to CDA 122, which has a high residual phosphorus content (0.02 wt%) [47]. Phosphorus solubility in copper is 0.5 wt% at 280°C, and is expected to decrease with decreasing temperature. Unfortunately, phosphorus-containing coppers, with concentrations of phosphorus greater than 0.004 wt%, have a known susceptibility to intergranular stress corrosion cracking (IGSCC) in ammonia environments [50]. (Ammonia formation may be possible under repository conditions because of microbial activity.) It has been suggested that IGSCC is caused by segregation of phosphorus to the grain boundaries [51]. The very limited solubility of phosphorus in copper could enhance this segregation at room temperature, where IGSCC has been observed. In the repository, however, the container temperature should initially remain relatively high. Perhaps the increased phosphorus solubility at the elevated temperatures will diminish its tendency to segregate to the grain boundaries and reduce the alloy's susceptibility to IGSCC.

## 5.2 CDA 715

CDA 715 is essentially a Cu-30 wt% Ni alloy with 0.5-wt% additions of iron and manganese (see Table 3). Manganese is the usual deoxidant in the alloy, and iron is added to increase corrosion resistance in moving seawater [46, 4]. The phase diagram for the binary alloy Cu-Ni [52–54] is shown in Fig. 19. For Cu-30Ni, the liquidus temperature is about 1240°C and the solidus temperature is about 1200°C. Copper and nickel have been found experimentally to be miscible at all compositions and temperatures, although at low temperatures, the diffusion of the constituent species is slow, and therefore the system approaches equilibrium very slowly.

Elford et al. [52] have predicted a miscibility gap for the copper-nickel alloy for temperatures less than 322°C (see Fig. 19), because the heat of formation of the solid alloys is positive. (However, these authors point out that a positive excess entropy may overcompensate for the positive heat of formation, in which case there would be no miscibility gap. This case is very rare with metallic solutions.) Under usual experimental conditions, the proposed miscibility gap is not expected to be seen because of the very slow approach to equilibrium at low temperatures. The waste-package container, as mentioned previously, is required to remain essentially intact for extended periods of time (300 to 1000 yr). The extent to which this alloy may approach the proposed phase separation is now considered.

The diffusion of the constituent species is the limiting step to the attainment of equilibrium. In particular, for the Cu-30Ni alloy, the diffusion of nickel in the copper lattice will be rate-determining. The diffusivity of nickel in bulk copper has been studied by numerous research groups [55–60]. The parameters to the best-fit equations for their experimental results are given in Table 4. Although the diffusivities were obtained at temperatures greater than those expected for the repository, estimates of relevant diffusivities were calculated by extrapolation to lower temperatures. However, note that such

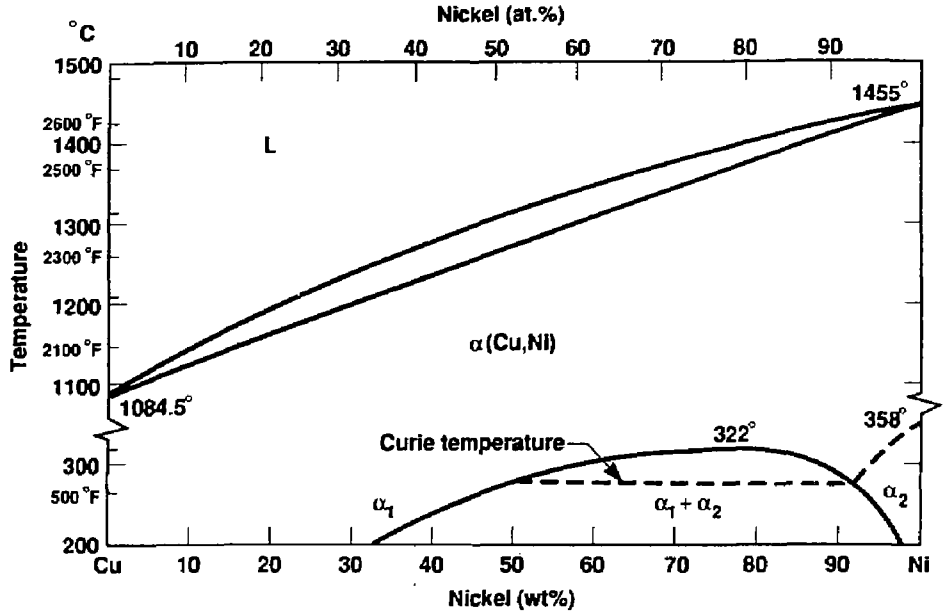


**Figure 19. Phase diagram for the copper-nickel system. The miscibility gap is proposed [52] but has not been experimentally observed.**

extrapolations are often underestimates because pipe and grain-boundary diffusion often dominate at low temperatures. Table 4 also lists calculated values of the diffusivities at 277, 177, and 77°C. The largest diffusivity is $6.4 \times 10^{-20}$ $cm^2/s$ at 277°C and $6.4 \times 10^{-24}$ $cm^2/s$ at 177°C. These values were calculated from the results given in Ref. 56 and are at least two orders of magnitude larger than those calculated from the other references.

Phase separation is proposed to occur in the Cu-30Ni alloy at temperatures below 200°C, with the nickel-rich phase having less than 5 wt% copper. Migration of nickel atoms in the copper matrix must occur for this phase separation to take place. An estimate of the nickel diffusion length, $x$, is obtained from

$$x^2 = 4Dt \qquad (3)$$

where $D$ is the diffusivity and $t$ is time.

In the repository, the expected maximum temperature is 250°C, and temperatures should remain above 150°C for 100 yr. The proposed miscibility gap is expected to form below 200°C for the Cu-30Ni alloy. A liberal estimate of the maximum diffusion length for the first 100 yr is obtained by assuming that the container temperature remains constant at 277°C for the entire time period. Using the maximum extrapolated diffusivity ($6.4 \times 10^{-20}$ $cm^2/s$), the calculated diffusion length is 0.3 μm ($3 \times 10^{-5}$ cm). Typical grain diameters in well-annealed metals are of the order of 10 μm. The calculated diffusion length of a nickel atom is about 3% of that diameter.

After the first 100 yr, the container temperature will be below 150°C. To estimate whether long times at these lower temperatures are sufficient for significant nickel precipitation to occur, it is assumed that the container temperature remains at 177°C. On the basis of the maximum calculated diffusivity ($6.4 \times 10^{-24}$ $cm^2/s$) and Eq. (3), the average nickel-atom diffusion length is calculated to be 0.009 μm ($9 \times 10^{-7}$ cm) in 1000 yr. This represents less than 0.1% of the grain diameter of a well-annealed metal. These calculations

Table 4. Best-fit parameters for the diffusivity of nickel in copper, and calculated diffusivities for nickel in copper at selected temperatures. The diffusivity $D$ is defined as $D_0 \exp(-E/RT)$, where $E$ is the activation energy for diffusion, $R$ is the gas constant, and $T$ is the temperature.

| $D_0$ ($cm^2/s$) | $E$ (kcal/mol) | Temp range (°C) | Calculated diffusivities ($cm^2/s$) 277°C | 177°C | 77°C | Ref. |
|---|---|---|---|---|---|---|
| 1.95 | 56.49 | 780–1040 | $7.0 \times 10^{-23}$ | $7.2 \times 10^{-28}$ | $5.3 \times 10^{-36}$ | 55 |
| 0.95 | 55.68 | 780–1040 | $7.1 \times 10^{-23}$ | $8.6 \times 10^{-28}$ | $1.6 \times 10^{-35}$ | 55[a] |
| 0.23 | 53.87 | 780–1040 | $9.0 \times 10^{-23}$ | $1.6 \times 10^{-27}$ | $5.3 \times 10^{-35}$ | 55[b] |
| 0.064 | 45.3 | 310–450 | $6.4 \times 10^{-20}$ | $6.4 \times 10^{-24}$ | $3.3 \times 10^{-30}$ | 56 |
| 0.8 | 53.7 | 500–900 | $3.7 \times 10^{-22}$ | $6.6 \times 10^{-27}$ | $2.4 \times 10^{-34}$ | 57 |
| 3.8 | 56.8 | 600–820 | $1.0 \times 10^{-22}$ | $9.9 \times 10^{-28}$ | $1.3 \times 10^{-35}$ | 58 |
| 1.93 | 55.6 | 855–1055 | $1.6 \times 10^{-22}$ | $3.7 \times 10^{-27}$ | $3.7 \times 10^{-35}$ | 59 |
| 2.7 | 56.5 | 700–1075 | $9.6 \times 10^{-23}$ | $9.8 \times 10^{-28}$ | $1.4 \times 10^{-35}$ | 60 |

[a] Cu, 1.08 at.% Ni.
[b] Cu, 2.81 at.% Ni.

suggest that the proposed phase separation will not occur to a significant extent during the containment time periods required of the metal canister in the repository. More extensive calculations should be performed to verify this simple analysis. The further analysis should include the effects of pipe and grain-boundary diffusion on the phase separation.

As mentioned above, 0.5 wt% of both manganese and iron are added to the Cu-30Ni alloy. Manganese at 0.5 wt% in copper is completely soluble at 200°C [61], and from extrapolation of the copper-manganese phase diagram (Fig. 20) it is expected to remain soluble to at least 0°C. Manganese in nickel at 0°C is expected to be soluble up to about 35 wt% manganese (see Fig. 21) [5]. Assuming that the properties of nickel and copper are additive and that copper and nickel themselves remain in solid solution, then manganese is expected to remain in solid solution in the alloy.

In contrast to manganese, iron is expected to be mostly insoluble in copper at temperatures less than 200°C. The solubility of iron in copper is less than 0.1% at 500°C [46] and decreases with decreasing temperature (see Fig. 22). In pure nickel, iron is expected to have limited solubility for temperatures less than 200°C (see Fig. 23). Some iron precipitation might occur because of this limited solubility; this may initially serve to precipitation-harden the alloy, though precipitation of large iron particles may adversely affect the alloy's corrosion properties. In the Cu-30Ni alloy, iron is usually dispersed uniformly by quenching from 900°C [46]. Iron is added to enhance the alloy's corrosion resistance in seawater, and in order to maintain its effectiveness it must remain dispersed throughout the bulk of the sample [1]. The iron in copper-nickel alloys is thought to form a hydrated iron oxide in the corrosion product, thereby improving its protective action.

In order to determine whether the iron diffusion rate is large enough to cause significant precipitation of iron, an analysis was performed similar to that done above for nickel in copper. Note that as before, the diffusivities at temperatures relevant to repository conditions were calculated by extrapolation from high temperatures. Also as before, diffusion mechanisms (pipe and grain-boundary) other than bulk diffusion tend to take over at low temperatures, giving larger diffusivities than those calculated by the above extrapolation. Table 5 gives best-fit parameters for the diffusivity of iron in copper and calculated diffusivities at selected temperatures. At 277°C, the iron diffusion length is 0.07 μm for the first 100 yr, and at 177°C, the

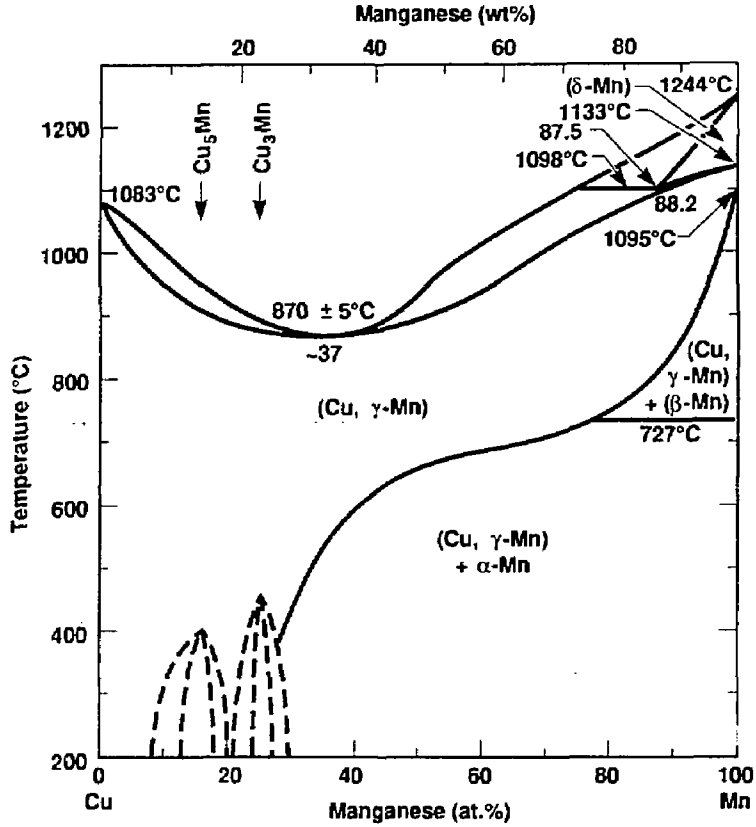


**Figure 20. Phase diagram for the copper-manganese system [5].**

diffusion length is 0.007 μm ($7 \times 10^{-7}$ cm) for a 1000-yr period. For both of these calculations, the largest calculated diffusivities were used. These diffusivities were at least 1 order of magnitude larger than most. In addition, the actual diffusivities may be even smaller because of the nickel component in the alloy. Calculated diffusivities of iron in pure nickel are nearly 5 orders of magnitude less than that used in the above calculations (see Table 6). For a well-annealed metal (grain diameter = 10 μm), the calculated diffusion lengths are less than 0.03 of an average grain diameter. On the basis of the above calculations, a significant amount of iron precipitation should not occur. Unless the corrosion resistance of the alloy is extremely sensitive to the iron atoms being finely dispersed throughout the lattice, it appears that the small amount of diffusion of iron should not adversely affect the alloy.

## 5.3 CDA 613

CDA 613 is a Cu-6.8 wt% Al alloy with the additional alloying elements Fe (2.5 wt%), Mn (0.2 wt%), and Sn (0.2 wt%). Manganese is soluble in copper at the temperatures of interest, as discussed previously. The solubility of tin in copper is very limited at repository temperatures, and its relevance is discussed later. Iron is insoluble in the alloy and forms metal particles that

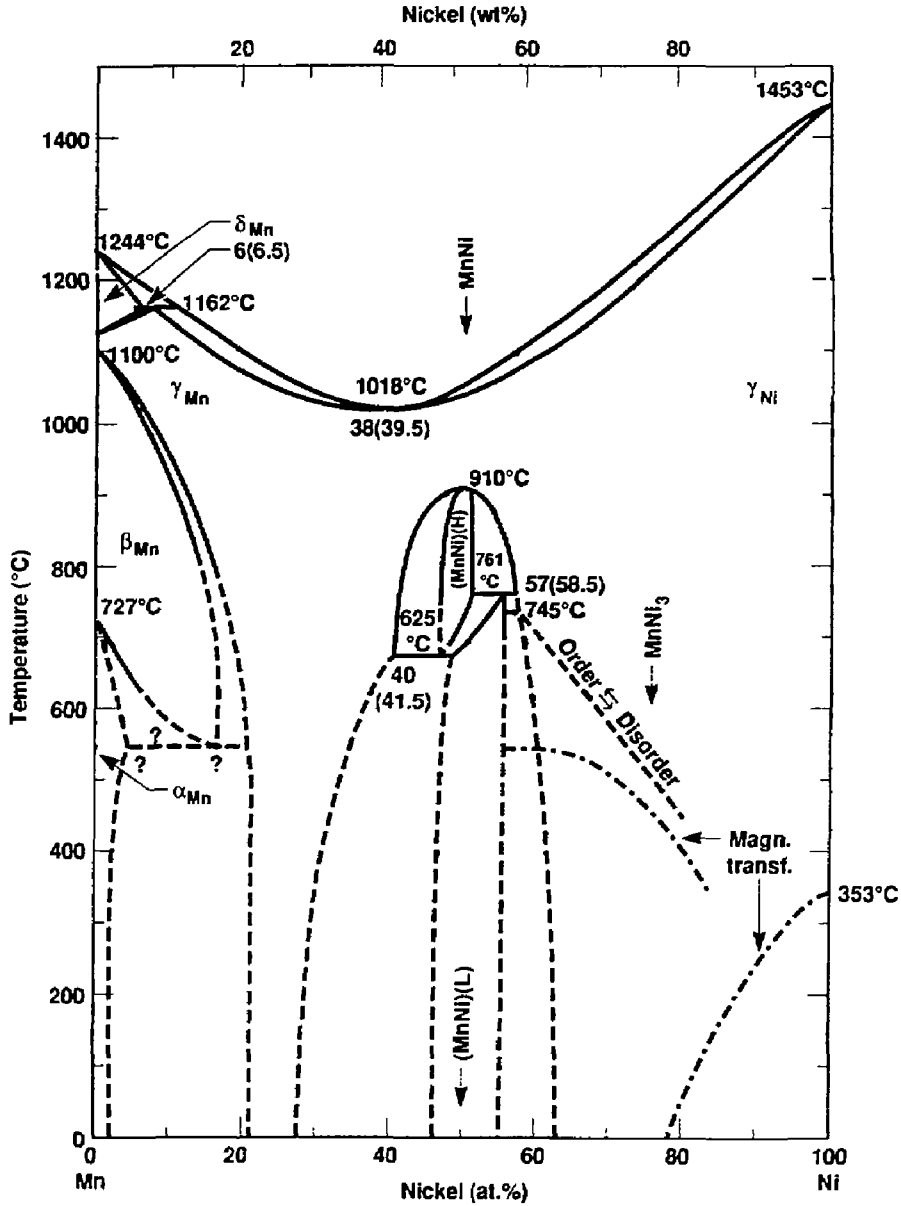


Figure 21. Phase diagram for the nickel-manganese system [5].

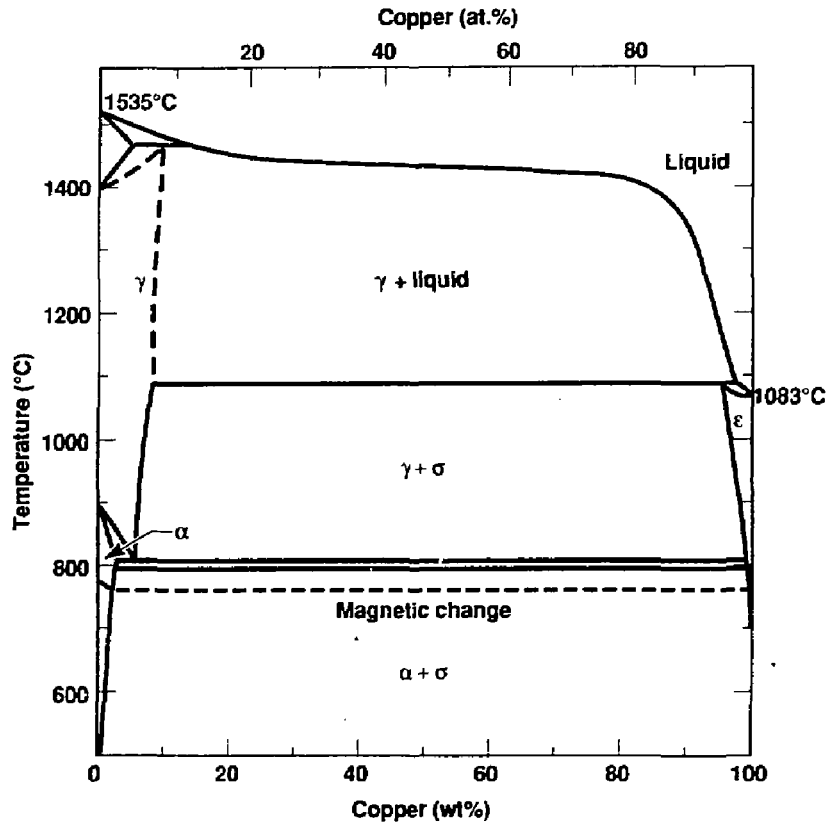


Figure 22. Phase diagram for the copper-iron system [62].

Table 5. Best-fit parameters for the diffusivity of iron in copper, and calculated diffusivities for iron in copper at selected temperatures.

| $D_0$ | $E$ | Temp range | Calculated diffusivities ($cm^2/s$) | | | |
|---|---|---|---|---|---|---|
| ($cm^2/s$) | (kcal/mol) | (°C) | 277°C | 177°C | 77°C | Ref. |
| 1.13 | 51.13 | 790–1000 | $5.4 \times 10^{-21}$ | $1.7 \times 10^{-25}$ | $1.3 \times 10^{-32}$ | 63 |
| 1.01 | 50.95 | 716–1056 | $5.7 \times 10^{-21}$ | $1.8 \times 10^{-25}$ | $1.5 \times 10^{-32}$ | 64 |
| 0.091 | 46.14 | 650–800 | $4.2 \times 10^{-20}$ | $3.6 \times 10^{-24}$ | $1.4 \times 10^{-30}$ | 65 |
| 1.4 | 51.8 | 700–1075 | $3.6 \times 10^{-21}$ | $9.8 \times 10^{-26}$ | $6.3 \times 10^{-33}$ | 60 |
| 1.3 | 51.5 | 732–1024 | $4.5 \times 10^{-21}$ | $1.3 \times 10^{-25}$ | $9.0 \times 10^{-33}$ | 66 |

harden the alloy [46]. As with the Cu-30Ni alloy, the diffusion of iron in the alloy needs to be considered. This will be discussed in more detail below. The phase diagram for the copper-rich end of the Cu-Al-3 wt% Fe alloy is shown in Fig. 24. At the composition Cu-6.8Al, the alloy is single-phased (α), with iron precipitates [Fe(δ)] down to least 300°C. It appears from the phase diagram that CDA 613 will remain single-phased for temperatures well below 300°C. Therefore,

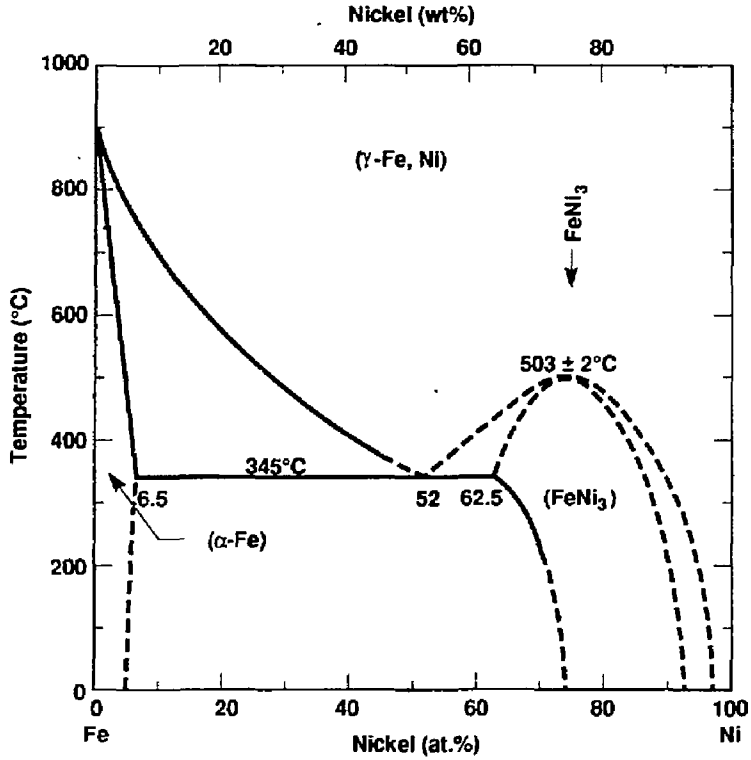


**Figure 23. Phase diagram for the iron-nickel system [5].**

**Table 6. Best-fit parameters for the diffusivity of iron in nickel, and calculated diffusivities for iron in nickel at selected temperatures.**

| $D_0$ | $E$ | Temp range | Calculated diffusivities ($cm^2/s$) | | | |
|---|---|---|---|---|---|---|
| ($cm^2/s$) | (kcal/mol) | (°C) | 277°C | 177°C | 77°C | Ref. |
| 0.22 | 60.4 | 1136–1356 | $2.2 \times 10^{-25}$ | $1.0 \times 10^{-30}$ | $4.2 \times 10^{-39}$ | 67 |
| 0.074 | 58.6 | 1020–1263 | $3.8 \times 10^{-25}$ | $2.6 \times 10^{-30}$ | $1.9 \times 10^{-38}$ | 68 |
| 1.0 | 64.2 | 1200–1400 | $3.1 \times 10^{-26}$ | $6.6 \times 10^{-32}$ | $8.2 \times 10^{-41}$ | 69 |
| 0.28 | 60.5 | 1140–1360 | $2.6 \times 10^{-25}$ | $1.2 \times 10^{-30}$ | $4.7 \times 10^{-39}$ | 70 |
| 0.0084 | 51.0 | 950–1130 | $4.6 \times 10^{-23}$ | $1.4 \times 10^{-27}$ | $1.2 \times 10^{-34}$ | 71 |

phase transformations do not appear to be a concern with this alloy.

The iron addition in this alloy is believed to be present in the form of the intermetallic compound $Fe_3Al$. These particles solution-harden the aluminum bronze alloy. In the intermetallic compound, iron diffusion is expected to be less than that of free iron in copper. However, since there are no data on the diffusion of the intermetallic compound, the diffusion of iron in this alloy is considered to be atomic for the sake of analysis. The simple analysis of the previous section

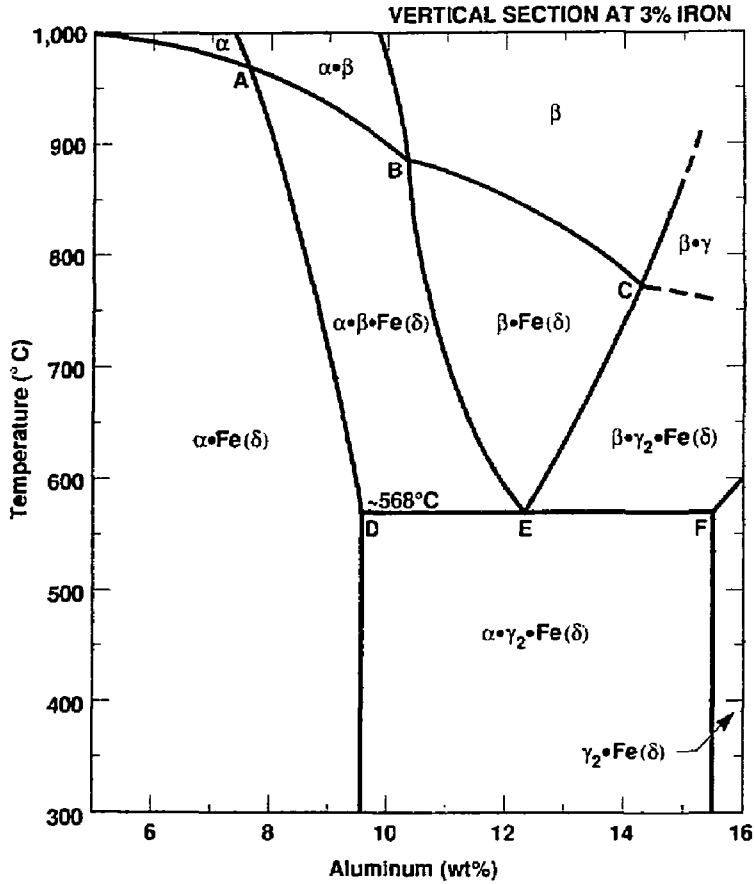


| | Point | | | | | |
|---|---|---|---|---|---|---|
| | A | B | C | D | E | F |
| °C | 970 | 885 | 770 | ~568 | ~568 | ~568 |
| Al (%) | 7.6 | 10.3 | ~14.3 | 9.5 | 12.3 | 15.5 |

**Figure 24. Phase diagram for the Cu-Al-3 wt% Fe system [46].**

indicates that iron diffusion in copper should be 3% of an average grain diameter of a well-annealed metal in the first 100 yr at 277°C, and 0.07% of an average grain diameter for a 1000-yr period at 177°C. These calculations indicate that iron diffusion and precipitation should not occur to a significant extent. More extensive calculations should be performed to more quantitatively show whether iron diffusion will be a problem.

A small amount (0.20 wt%) of tin is added to CDA 613 in order to reduce its susceptibility to IGSCC in steam environments [72]. The enhanced resistance is thought to be due to tin segregation to grain boundaries. This is discussed more fully in Volume 4 of this report [1]. Tin is soluble in copper up to 0.74 wt% at 170°C, and the solubility decreases to zero near 100°C [5]. At the initial high temperature of the repository, the tin

should remain in solution. As the temperature decreases, there is the possibility of precipitation of the tin. A diffusion analysis similar to that carried out in the previous sections is now applied to this situation. Data for high-temperature bulk diffusion are used to obtain diffusion lengths at low temperatures. Again, this will underestimate the diffusion lengths as other diffusion paths (grain-boundary and pipe) predominate at low temperatures. Measured diffusion values vary little among published studies [73–75]. The average activation energy for tin diffusion in copper is 44.6 kcal/mol, and the average pre-exponential is 0.78 $cm^2/s$. To obtain a liberal estimate of the average tin diffusion length in the lower-temperature region, it is assumed that the copper temperature is 177°C for 1000 yr. The calculated diffusion length is 0.05 μm. This length is sufficiently small that tin precipitation should not occur to a significant extent.

## 6. Summary of the Survey of Copper-Based Alloys

A review of the literature with respect to the phase stability of the copper-based candidate materials CDA 102, CDA 613, and CDA 715 has been completed. According to the available experimental data, all of the candidate materials are single-phased to at least 300°C. There is a proposed two-phase region for CDA 715 at temperatures less than 200°C, but constituent diffusion rates are so slow at the expected repository temperatures that a phase transformation does not appear likely.

The migration of iron in both CDA 613 and CDA 715 and the migration of tin in CDA 613 may be potential problems in these materials. Mechanical properties in CDA 613 and corrosion properties in CDA 715 rely on small iron particles being uniformly dispersed throughout the bulk. Calculations indicate that the diffusion length of iron should be small under the expected repository conditions, but it is not known what the potential degradation of the material properties could be for the perturbation of the iron-particle distribution. Tin remains soluble in copper to much lower temperatures (<170°C) than does iron. At these lower temperatures, not much diffusion is expected, and precipitation of tin is not expected to be significant. More extensive calculations and experiments are advised to determine the possibility of constituent precipitation and its possible detrimental effects.

## 7. Ranking of the Copper-Based Candidate Alloys

Considering only the phase stability of the three copper-based alloys, the following ranking is proposed:

1. CDA 102
2. CDA 613 and CDA 715

CDA 102 is ranked first because it is essentially pure copper and is single-phased. CDA 613 and CDA 715 are also known to be single-phased at high temperature, but they are ranked lower than CDA 102 for two reasons. (1) There may be an unknown phase transition that occurs at the expected repository temperatures after extended time periods. (2) Migration and precipitation of iron (CDA 715 and CDA 613) and tin (CDA 613) may occur in the bulk and cause material degradation. Preliminary calculations indicate that these effects may not be significant, but more extensive modeling and experimentation are suggested.

## 8. Acknowledgments

This work was performed under the auspices of the U.S. Department of Energy by Lawrence Livermore National Laboratory under contract No. W-7405-ENG-48, and was supported by the Yucca Mountain Project.

# 9. References


1. G. E. Gdowski, D. B. Bullen, *Survey of Degradation Modes of Candidate Materials for High-Level Radioactive-Waste Disposal Containers, Vol. 2, Oxidation and Corrosion*, Lawrence Livermore National Laboratory, Livermore, California, UCID-21362 Vol. 2 (1988). NN1.881220.0036

   J. C. Farmer, R. A. Van Konynenburg, R. D. McCright, D. B. Bullen, *Survey of Degradation Modes of Candidate Materials for High-Level Radioactive-Waste Disposal Containers, Vol. 3, Localized Corrosion and Stress Corrosion Cracking of Austenitic Alloys*, Lawrence Livermore National Laboratory, Livermore, California, UCID-21362 Vol. 3 (1988). NN1.881220.0037

   J. C. Farmer, R. A. Van Konynenburg, R. D. McCright, G. E. Gdowski, *Survey of Degradation Modes of Candidate Materials for High-Level Radioactive-Waste Disposal Containers, Vol. 4, Stress Corrosion Cracking of Copper-Based Alloys*, Lawrence Livermore National Laboratory, Livermore, California, UCID-21362 Vol. 4 (1988). NN1.881220.0038

   J. C. Farmer, R. D. McCright, R. A. Van Konynenburg, G. E. Gdowski, *Survey of Degradation Modes of Candidate Materials for High-Level Radioactive-Waste Disposal Containers, Vol 5, Localized Corrosion of Copper-Based Alloys*, Lawrence Livermore National Laboratory, Livermore, California, UCID-21362 Vol. 5 (1988). NN1.881220.0039

   G. E. Gdowski, D. B. Bullen, *Survey of Degradation Modes of Candidate Materials for High-Level Radioactive-Waste Disposal Containers, Vol. 6, Effects of Hydrogen in Austenitic and Copper-Based Alloys*, Lawrence Livermore National Laboratory, Livermore, California, UCID-21362 Vol. 6 (1988). NN1.881220.0040

   M. J. Strum, H. Weiss, J. C. Farmer, D. B. Bullen, *Survey of Degradation Modes of Candidate Materials for High-Level Radioactive-Waste Disposal Containers, Vol. 7, Weldability of Austenitic Alloys*, Lawrence Livermore National Laboratory, Livermore, California, UCID-21362 Vol. 7 (1988). NN1.881220.0041

   D. B. Bullen, G. E. Gdowski, H. Weiss, *Survey of Degradation Modes of Candidate Materials for High-Level Radioactive-Waste Disposal Containers, Vol. 8, Weldability of Copper-Based Alloys*, Lawrence Livermore National Laboratory, Livermore, California, UCID-21362 Vol. 8 (1988). NN1.881220.0042

2. C. J. Novak, "Structure and Constitution of Wrought Austenitic Stainless Steels," in *Handbook of Stainless Steels*, D. Peckner and I. M. Bernstein, Eds., McGraw-Hill Book Co., New York, 1977, Chapter 4. NNA.891009.0002
3. P. Marshall, *Austenitic Stainless Steels*, Elsevier Publishers, London, 1984. NNA.891026.0019
4. W. Betteridge, *Nickel and its Alloys*, John Wiley and Sons, New York, 1984. NNA.891009.0003
5. M. Hansen, K. Anderko, *Constitution of Binary Alloys*, 2nd Ed., McGraw-Hill, New York, 1958. NNA.891009.0004
6. E. C. Bain, R. H. Aborn, in *Metals Handbook*, American Society for Metals, Metals Park, Ohio, 1948, p. 1261.
7. J. W. Pugh, J. D. Nisbet, "Iron-Chromium-Nickel Ternary System," *Journal of Metals, Transactions AIME*, Vol. 188, February 1950, pp. 268–276. NNA.891009.0005
8. G. R. Speich, in *Metals Handbook*, American Society for Metals, Metals Park, Ohio, Vol. 8, 1973, p. 425. NNA.891009.0006
9. H. Schneider, "Investment Casting of High-hot-strength 12-per-cent. Chrome Steel," *Foundry Trade Journal*, Vol. 108, 1960, p. 562. NNA.891009.0007
10. H. D. Harries, *International Conference on the Mechanical Behavior and Nuclear Applications of Stainless Steel at Elevated Temperatures, Varese, May 1981*, Metals Society, London. NNA.891026.0017
11. F. C. Hull, "Delta Ferrite and Martensite Formation in Stainless Steels," *Welding Journal*, Vol. 52, No. 5, May 1973, pp. 193s–203s. NNA.891009.0008

12. H. S. Avery, U.S. Patent 2, 465,780, January 1974. NNA.891018.0175
13. H. C. Campbell, R. D. Thomas, "The Effect of Alloying Elements on the Tensile Properties of 25-20 Weld Metal," *Welding Journal, Welding Research Supplement*, Vol. 25, 1946, p. 760s. NNA.891009.0009
14. A. L. Schaeffler, "Constitution Diagram for Stainless Steel Weld Metal," *Metal Progress*, Vol. 56, No. 5, November 1949, p. 680. NNA.891009.0010
15. W. T. DeLong, "A Modified Phase Diagram for Stainless Steel Weld Metals," *Metal Progress*, Vol. 77, No. 2, February 1960, pp. 98–100. NNA.891009.0011
16. H. C. Campbell, "The Ferrite Problem—Is It a Tempest in a Teapot?" *Welding Journal*, Vol. 54, No. 12, December 1975, pp. 867–871. NNA.891009.0012
17. H. M. Otte, "The Formation of Stacking Faults in Austenite and Its Relation to Martensite," *Acta Metallurgica*, Vol. 5, November 1957, pp. 614–627. NNA.891009.0013
18. G. Krauss, A. R. Marder, "The Morphology of Martensite in Iron Alloys," *Metallurgical Transactions*, Vol. 2, September 1971, pp. 2343–2357. NNA.891009.0014
19. R. P. Reed, J. F. Breedis, "Low-Temperature Phase Transformations," in *Behavior of Metals at Cryogenic Temperatures*, American Society for Testing and Materials, Philadelphia, Pennsylvania, ASTM Special Technical Publication 387 (1966), pp. 60–132. NNA.891009.0015
20. J. F. Breedis, "Martensitic Transformations in Iron-Chromium-Nickel Alloys," *Metallurgical Society, Transactions AIME*, Vol. 230, No. 7, December 1964, pp. 1583–1596. NNA.891009.0016
21. J. A. Venables, "The Martensite Transformation in Stainless Steel," *Philosophy Magazine*, Vol. 7, 1962, pp. 35–44. NNA.891009.0017
22. J. Dash, H. M. Otte, "The Martensite Transformation in Stainless Steel," *Acta Metallurgica*, Vol. 11, October 1963, pp. 1169–1178. NNA.891009.0018
23. B. Cina, "Effect of Cold Work on the $\gamma$–$\alpha$ Transformation in Some Fe-Ni-Cr Alloys," *Journal of the Iron and Steel Institute*, Vol. 177, August 1954, pp. 406–422. NNA.891009.0019
24. R. P. Reed, "The Spontaneous Martensitic Transformations in 18%Cr, 8%Ni Steels," *Acta Metallurgica*, Vol. 10, September 1962, pp. 865–877. NNA.891009.0020
25. J. F. Breedis, W. D. Robertson, "The Martensitic Transformation in Single Crystals of Iron-Chromium-Nickel Alloys," *Acta Metallurgica*, Vol. 10, November 1962, pp. 1077–1088. NNA.891009.0021
26. V. Cihal (Chigal), "Intercrystalline Corrosion of Corrosion Resistant Steels," *Protection of Metals*, Vol. 4, No. 6, November-December 1968, pp. 563–577. NNA.891009.0022
27. R. Stickler, A. Vinckier, "Morphology of Grain-Boundary Carbides and Its Influence on Intergranular Corrosion of 304 Stainless Steel," *Transactions American Society for Metals*, Vol. 54, 1961, pp. 362–380. NNA.891009.0023
28. B. Weiss, R. Stickler, "Phase Instabilities During High Temperature Exposure of 316 Austenitic Stainless Steel," *Metallurgical Transactions*, Vol. 3, April 1972, pp. 851–866. NNA.891009.0024
29. C. Da Casa, V. B. Nileshwar, D. A. Melford, "$M_{23}C_6$ Precipitation in Unstabilized Austenitic Stainless Steel," *Journal of the Iron and Steel Institute*, London, Vol. 207, 1969, pp. 1325–1332. NNA.891009.0025
30. J. A. Spitznagel, R. Stickler, "Correlation Between Precipitation Reactions and Bulk Density Changes in Type 18-12 Austenitic Stainless Steels," *Metallurgical Transactions*, Vol. 5, June 1974, pp. 1363–1371. NNA.891009.0026
31. C. J. Bechtoldt, H. C. Vacher, "Phase-Diagram Study of Alloys in the Iron-Chromium-Molydenum-Nickel System," *Journal of Research of the National Bureau of Standards*, Vol. 58, No. 1, January 1953, pp. 7-19. NNA.891009.0027
32. E. C. Bain, W. E. Griffiths, "An Introduction to the Iron-Chromium-Nickel Alloys," *Transactions AIME*, Vol. 75, 1972, pp. 166–213. NNA.891009.0028
33. A. M. Talbot, D. E. Furman, "Sigma Formation and Its Effect on the Impact Properties of Iron-Nickel-Chromium Alloys," *Transactions of the A.S.M.*, Vol. 45 1942, p. 429. NNA.891009.0029
34. M. Henthorne, "Intergranular Corrosion in Iron and Nickel Base Alloys," *Localized Corrosion—Cause of Metal Failure*, American Society for Testing and Materials, Philadelphia, Pennsylvania, ASTM Special Technical Publication 516 (1972), pp. 66–119. NNA.891009.0030
35. M. H. Brown, R. W. Kirchner, "Sensitization of Wrought High Nickel Alloys," *Corrosion*, Vol. 29, No. 12, December 1973, pp. 470–474. NNA.891009.0031

36. M. H. Brown, "The Relationship of Heat Treatment to the Corrosion Resistance of Stainless Alloys," *Corrosion*, Vol. 25, No. 10, October 1969, pp. 438–443. NNA.891009.0032
37. H. R. Copson, B. E. Hopkinson, F. S. Lang, "Behavior of Ni-O-Nel Nickel-Iron-Chromium Alloy in Intergranular Corrosion Evaluation Tests," *Proceedings ASTM*, Vol. 61, 1961, pp. 879–889. NNA.891009.0033
38. E. L. Raymond, "Mechanisms of Sensitization and Stabilization of Incoloy Nickel-Iron-Chromium Alloy 825," *Corrosion*, Vol. 24, No. 6, June 1968, pp. 180–188. NNA.891009.0034
39. C. T. Sims, "A Contemporary View of Nickel-Base Superalloys," *Journal of Metals*, Vol. 18, October 1966, pp. 1119–1130. NNA.891009.0035
40. C. P. Sullivan, M. J. Donachie, "Some Effects of Microstructure on the Mechanical Properties of Nickel-Base Superalloys," *Metals Engineering Quarterly*, Vol. 7, No. 2, February 1967, pp. 36–45. NNA.891009.0036
41. C. P. Sullivan, M. J. Donachie, "Microstructures and Mechanical Properties of Iron-Base (-Containing) Superalloys," *Metals Engineering Quarterly*, Vol. 11, No. 4, November 1971, pp. 1–11. NNA.891009.0037
42. D. R. Muzyka, "Controlling Microstructures and Properties of Superalloys Via Use of Precipitated Phases," *Metals Engineering Quarterly*, Vol. 11, No. 4, November 1971, pp. 12–20. NNA.891009.0038
43. R. T. Holt, W. Wallace, "Impurities and Trace Elements in Nickel-Base Superalloys," *International Metals Reviews*, Vol. 21, No. 203, March 1976, pp. 1–24. NNA.891009.0039
44. G. Chen, X. Xie, K. Ni, Z. Xu, D. Wang, M. Zhang, Y. Ju, "Grain Boundary Embrittlement by μ and α Phases in Iron-Base Superalloys," in *Superalloys 1980*, American Society for Metals, Metals Park, Ohio, 1980, pp. 323–333. NNA.891009.0040
45. R. D. McCright, *FY 1985 Status Report on Feasibility Assessment of Copper Base Waste Package Container Materials in a Tuff Repository*, Lawrence Livermore National Laboratory, Livermore, California, UCID-20509 (September 30, 1985). HQS.880517.2492
46. E. G. West, *Copper and Its Alloys*, John Wiley and Sons, New York, 1982.
47. *Metals Handbook, Volume 2, Properties and Selection: Nonferrous Alloys and Pure Metals*, 9th ed., American Society for Metals, Metals Park, Ohio, 1979, pp. 237–490. NNA.891009.0041
48. T. A. Ramanarayanan, W. L. Worrell, "Overvoltage Phenomena in Electrochemical Cells with Oxygen-Saturated Copper Electrodes," *Metallurgical Transactions*, Vol. 5, August 1974, pp. 1773–1777. NNA.891009.0042
49. M. L. Narula, V. B. Tare, W. L. Worrell, "Diffusivity and Solubility of Oxygen in Solid Copper Using Potentiostatic and Potentiometric Techniques," *Metallurgical Transactions*, Vol. 14B, December 1983, pp. 673–677. NNA.891009.0067
50. D. H. Thompson, A. W. Tracy, "Influence of Composition on the Stress-Corrosion Cracking of Some Copper-Base Alloys," *The Journal of Metals*, Vol. 1, February 1949, pp. 100–109. NNA.891018.0173
51. H. H. Uhlig, D. J. Duquette, "Alleged Stress-Corrosion Cracking of Pure Copper," *Corrosion Science*, Vol. 19, 1969, pp. 557–560. NNA.891009.0043
52. L. Elford, F. Muller, O. Kubaschewski, "The Thermodynamic Properties of Copper-Nickel Alloys," *Berichte der Bunsengesellschaft*, Vol. 73, No. 6, 1969, pp. 601–605. NNA.891009.0044
53. E. A. Feest, R. D. Doherty, "The Cu-Ni Equilibrium Phase Diagram," *Journal of the Institute of Metals*, Vol. 99, 1971, pp. 102–104.
54. V. E. Schurmann, E. Schulz, "Untersuchungen zum Verlauf der Liquidus- und Soliduslinien in den Systemen Kupfer-Mangan und Kupfer-Nickel," *Zeitschrift für Metallkunde*, Vol. 62, 1971, pp. 758–763. NNA.891009.0045
55. M. B. Dutt, S. K. Sen, A. K. Barua, "The Diffusion of Nickel into Copper and Copper-Nickel," *Physica Status Solidi A*, Vol. 56, 1979, pp. 149–155. NNA.891009.0046
56. H. P. Bonzel, "Diffusion of Ni-63 in Alpha-Irradiated Copper," *Acta Metallurgica*, Vol. 13, 1965, pp. 1084–1086. NNA.891009.0047
57. J. -L. Seran, "Etude de l'effet isotopique pour la diffusion du nickel dans le cuivre par spectrometries de masse a emission ionique secondaire," *Acta Metallurgica*, Vol. 24, 1976, pp. 627–631. NNA.891009.0048
58. A. J. Ikushima, "Diffusion of Nickel in Single Crystals of Copper," *Journal of the Physical Society of Japan*, Vol. 14, 1959, p. 1636. NNA.891009.0049

59. K. J. Anusavice, J. J. Pinajin, H. Oikawa, R. T. Dehoff, "Utilization of Ni-66 in Tracer Diffusion Studies," *Transactions AIME*, Vol. 242, 1968, p. 2027. NNA.891009.0050
60. C. A. Mackliet, "Diffusion of Iron, Cobalt, and Nickel in Single Crystals of Pure Copper," *Physical Review*, Vol. 109, No. 6, March 1958, pp. 1964-1970. NNA.891009.0051
61. *Constitution of Binary Alloys, Second Supplement*, F. A. Shunk, Ed., McGraw-Hill, New York, 1969. NNA.891009.0052
62. *Smithhells Metals Reference Book*, 6th ed., E. A. Brandes, Ed., Butterworths, London, 1983. NNA.891009.0053
63. S. K. Sen, M. B. Dutt, A. K. Barua, "The Diffusion of Iron in Copper and of Nickel in Silver," *Physica Status Solidi A*, Vol. 45, 1978, pp. 657–663. NNA.891009.0054
64. J. G. Mullen, "Isotope Effect in Intermetallic Diffusion," *Physical Review*, Vol. 121, No. 6, March 1961, pp. 1649–1658. NNA.891009.0055
65. G. Salje, M. Feller-Kniepmeier, "The Diffusion and Solubility of Iron in Copper," *Journal of Applied Physics*, Vol. 49, No. 1, January 1978, pp. 229–232. NNA.891009.0056
66. J. Bernardini, J. Cabane, "Influence des dislocations sur la cinetique de diffusion du fer, du cobalt et du ruthenium dans le cuivre et l'argent monocristallins," *Acta Metallurgica*, Vol. 21, December 1973, pp. 1561–1569. NNA.891009.0057
67. M. Badia, A. Vignes, "Diffusion du Fer, du Nickel et du Cobalt dans les Metaux de Transition du Groupe du Fer," *Acta Metallurgica*, Vol. 17, February 1969, pp. 177–187. NNA.891009.0058
68. A. Ya. Shinyaev, "Diffusion in Nickel-Iron Alloys," *Izv. Akad. Nauk. SSSR, Metl.*, Vol. 4, 1969, p. 262. NNA.891009.0059
69. H. Bakker, J. Backus, F. Waals, "Curvature in the Arrhenius Plot for the Diffusion of Iron in Single Crystals of Nickel in the Temperature Range 1200-1400°C," *Physica Status Solidi B*, Vol. 45, 1971, pp. 633–638. NNA.891009.0060
70. M. Badia, A. Vignes, "Diffusion in the Iron-Nickel System," *C. R. Acad. Sci., Paris, Series C*, Vol. 264, May 1967, pp. 1528–1531. NNA.891009.0061
71. M. B. Neimann, A. Y. Shinyaev, B. G. Dzantiev, "Diffusion of Iron in Nickel," *Dok. Akad. Nauk. SSSR*, Vol. 91, 1953, pp. 265–267. NNA.891009.0062
72. J. F. Klement, R. E. Maersch, P. A. Tully, "Use of Alloy Additions to Prevent Intergranular Stress Corrosion Cracking in Aluminum Bronze," *Corrosion*, Vol. 16, No. 10, October 1960, pp. 519t–522t. NNA.891009.0063
73. G. Krautheim, A. Neidhardt, U. Reinhold, A. Zehe, "Activation Energy Differences for Impurity Diffusion of $V^{th}$ Period Elements in Copper," *Solid State Communications*, Vol. 34, No. 3, 1980, pp. 163–166. NNA.891009.0064
74. V. A. Gorbachev, S. M. Klotsman, Ya. A. Rabovsky, V. K. Talinsky, A. N. Timofeev, *Fiz. Met. Metalloved*, Vol. 35, No. 4, 1973, pp. 889–892. NNA.891009.0065
75. R. L. Fogelson, Ya. A. Ugay, I. A. Akimova, "Diffusion of Tin in Copper," *Fiz. Met. Metalloved*, Vol. 37, No. 5, 1974, pp. 1107–1108. NNA.891009.0066

The following number is for Office of Civilian Radioactive Waste Management Records Management purposes only and should not be used when ordering this document:

Accession Number: NNA.891222.0306